

# Cyclic activity of Fuego de Colima volcano (Mexico): insights from satellite thermal data and non-linear models

Silvia Massaro<sup>1,2\*</sup>, Antonio Costa<sup>2</sup>, Roberto Sulpizio<sup>1,3</sup>, Diego Coppola<sup>4</sup>, Lucia Capra<sup>5</sup>

<sup>1</sup>Istituto per la Dinamica dei Processi Ambientali – Consiglio Nazionale delle Ricerche, Via R. Cozzi 53, 20125, Milan (Italy)

<sup>2</sup>Istituto Nazionale di Geofisica e Vulcanologia, Via D. Creti 12, 40128, Bologna (Italy)

<sup>3</sup>Dipartimento di Scienze della Terra e Geoambientali, Università di Bari, Via Orabona 4, 70125, Bari (Italy)

<sup>4</sup>Dipartimento di Scienze della Terra, Università di Torino, Via Valperga Caluso, 35, 10129, Turin (Italy)

<sup>5</sup>Centro de Geociencias UNAM, Campus Juriquilla, Queretaro (Mexico)

\*Corresponding Author: Silvia Massaro (silvia-massar@libero.it)

## Abstract

The Fuego de Colima volcano (Mexico) shows a complex eruptive behaviour with periods of rapid and slow lava dome growth, punctuated by explosive activity. We reconstructed the weekly discharge rate average between 1998 and 2018 by means of satellite thermal data integrated with published discharge rate data. By using spectral and wavelet analysis, we found a multi-year long-, multi-month intermediate-, and multi-week short-term cyclic behaviour during the period of the investigated eruptive activity, as those of many others dome-forming volcanoes. We use numerical modelling in order to investigate the non-linear cyclic eruptive behaviour considering a magma feeding system composed of a dual or a single magma chamber connected to the surface through an elastic dyke developing into a cylinder conduit in the shallowest part. We investigated the cases in which the periodicity is controlled by i) the coupled deep-shallow magma reservoirs, ii) the single shallow chamber, and iii) the elastic shallow dyke when is fed by a fixed influx rate or a constant pressure. Due to the limitations of the current modelling approach, there is no single configuration that can reproduce all the periodicities on the three different time scales. The model outputs indicate that the observed multi-year periodicity (1.5-2.5 years) can be described by the fluctuations controlled by a shallow magma chamber with a volume of 20-50 km<sup>3</sup> coupled with a deep reservoir of ca. 500 km<sup>3</sup>, connected through a deep elastic dyke. The multi-month periodicity (ca. 5 - 10 months) appears to be controlled by the shallow magma chamber for the same range of volumes. The short-term multi-week periodicity (ca. 2.5 - 5 weeks) can be reproduced considering a fixed influx rate or constant pressure at the base of the shallower dyke. This work provides new insights on the non-linear cyclic behaviour of Fuego de Colima, and a general framework for the comprehension of eruptive behaviour of andesitic volcanoes.

## 37 **1. Introduction**

38 Lava dome forming eruptions are relatively long-lived events, lasting from several months to  
39 several decades (e.g. Merapi, Indonesia, Siswamidjono et al., 1995; Kelut, Indonesia, De Bézizal et  
40 al., 2012; Fuego de Colima, Mexico, Lamb et al., 2014; Santiaguito, Guatemala, Harris et al.,  
41 2002), and usually punctuated by dome collapses and explosive (Vulcanian) episodes. Discharge  
42 rates can change widely over a range of time scales, reflecting the physical mechanisms involved in  
43 the transfer of magma to the Earth's surface (Melnik et al., 2008; Odbert and Wadge, 2009). Dome  
44 growth shows a periodic behaviour, which has been commonly observed at several volcanoes,  
45 including Santiaguito (Guatemala, Harris et al., 2003), Mt St Helens (USA, Swanson and Holcomb,  
46 1990), and Soufrière Hills (Montserrat, Voight et al., 1998; Loughlin et al., 2010; Wadge et al.,  
47 2010; Nicholson et al., 2011). Periodic behaviours can be complex, showing systematic or non-  
48 systematic temporal changes as the eruption progresses (Denlinger and Hoblitt, 1999; Costa et al.,  
49 2007a; Melnik et al., 2008; Bernstein et al., 2013; Wolpert et al., 2016), and can be characterized by  
50 short-, intermediate- and long-term periodicities (Costa et al., 2007a; Melnik et al., 2008; Costa et  
51 al., 2012; 2013; Melnik and Costa, 2014). Short- and intermediate-term periodicities (hours or  
52 weeks) are generally explained by the upper conduit pressurization related to the non-linear ascent  
53 of magma flow (Denlinger and Hoblitt, 1999; Melnik and Sparks, 1999; Voight et al., 1999; Wylie  
54 et al., 1999; Ozerov et al., 2003; Lensky et al., 2004, Costa et al., 2007a,b; 2012; Kozono and  
55 Koyaguchi, 2009; 2012). This is because the lower part of the dyke-conduit can act as a capacitor  
56 that allows magma to be stored temporarily and released during the more intense phase of discharge  
57 (Costa et al., 2007a,b; Melnik et al., 2008; Costa et al. 2012; 2013). The long-term periodicity, with  
58 time scales from several months to decades (Voight et al., 2000; Belousov et al., 2002; Sparks and  
59 Young, 2002; Wadge et al., 2006), is usually controlled by pressure variations in magma reservoirs  
60 (Barmin et al., 2002; Costa et al., 2007b; Melnik et al., 2008; Melnik and Costa, 2014). Since  
61 historical times, the Fuego de Colima volcano (Mexico; Fig.1a) has been characterised by decade-  
62 lasting cycles of dome growth alternating with Vulcanian explosions, ended with sub-Plinian

63 eruptions (the last two occurred in 1818 and 1913; Luhr, 2002; Saucedo et al., 2005; Norini et al.,  
64 2010; Heap et al., 2014; Massaro et al., 2018a). The most recent cycle started after the 1913  
65 eruption, and it is characterized by lava domes extruded with minor seismicity at high magma  
66 temperatures (960-1020°C; Savov et al., 2008). As for other dome eruptions (Sparks, 1997), dome  
67 growth at Fuego de Colima can be explained by complex non-linear pressure variations during  
68 magma ascent from magma reservoirs (e.g. Melnik and Costa, 2014), cooling, crystallization,  
69 degassing (e.g. Melnik and Sparks, 1999; Lensky et al., 2004; Nakanishi and Koyaguchi, 2008;  
70 Kozono and Koyaguchi, 2012) and upper conduit geometric configurations characterized by  
71 multiple pathways (e.g. Lavallée et al., 2012; Reubi et al., 2015).

72 Two magma chambers located at different depths characterize the feeding system of Fuego de  
73 Colima volcano (Fig. 1b), with roofs located at ca. 6 (shallow magma chamber) and ca. 15 km  
74 (deep magma chamber) of depth, as indicated by petrographic studies (Macias et al., 2017) and  
75 geophysical data (Spica et al., 2017).

76 The purpose of this study is to investigate the existence of pattern of fluctuations in discharge rates  
77 during the 1998-2018 erupted activity at Fuego de Colima volcano. The available geological,  
78 geophysical, and petrological data for this recent activity provide a remarkable opportunity to  
79 improve the characterization and our understanding about the physical processes underlying cyclic  
80 extrusion of lava domes. In particular, we used thermal remote sensing data along with published  
81 effusion rates for reconstructing the oscillatory magma discharge rate behaviour of effusive activity  
82 at Colima.

83 The availability of satellite thermal images in the last decade has strengthened the use of thermal  
84 data for observing volcanic activity (e.g. Ramsey and Harris, 2012), especially in studying the  
85 relationships with lava discharge rates (Coppola et al., 2009; Harris et al., 2010; Garel et al., 2012).  
86 Coppola et al. (2013) propose that the radiant density of effusive/extrusive activity can be used to  
87 estimate lava discharge rates and erupted volumes by means of empirical relationship based on SiO<sub>2</sub>  
88 content of the erupted lava. Although it is still under debate, the so-called “thermal approach”

89 (Dragoni and Tallarico, 2009) offers a good way for monitoring volcanic activity, especially when  
90 direct observations are limited or absent. Here we focus our attention to the dynamics of  
91 fluctuations in magma discharge rate at different timescales at Fuego de Colima volcano during  
92 1998-2018. By using time series analytical techniques (i.e. Fourier and wavelet analysis) we have  
93 identified three fundamental periodicities in subsets of the time series: i) long-term (ca. 1.5-2.5  
94 years), ii) intermediate-term (ca. 5-10 months), iii) short-term (ca. 2.5-5 weeks), similar to those  
95 observed at many lava-dome eruptions (e.g. Costa et al., 2012; Melnik and Costa, 2014; Christopher  
96 et al., 2015). These periodicities were compared with numerical simulations provided by the model  
97 of Melnik and Sparks (2005) as generalized by Costa et al. (2007a) for accounting the presence of a  
98 shallow dyke, and Melnik and Costa (2014) for describing the control of a coupled dual chamber  
99 system. Numerical modelling of the different parts of the plumbing system can successfully  
100 reproduce the first-order cyclic behaviour of Fuego de Colima during the 1998-2018 erupted  
101 activity. Our results highlight that the dual magma chamber dynamics controls the long-term  
102 periodicity evident during 2002-2006 and 2013-2016, while the single magma chamber dynamics  
103 are more effective to explain the intermediate-term periodicity in the same periods. Finally, the  
104 shallow dyke dynamics regulate the multi-week cycles observed during 2002-2006 and 2011-2016.  
105 The present work is divided in five main sections. The first describes the historical activity of the  
106 Fuego de Colima, with particular attention to the recent period, from 1998 to 2018. The second  
107 section describes the methods applied to the dataset composed of the satellite thermal data  
108 integrated with published data. The third section is dedicated to the input and target data used for  
109 numerical simulations. The fourth section presents the results obtained by the spectral and wavelet  
110 analyses. This latter allows us to establish significance levels for the wavelet power spectrum. The  
111 periodicities observed in this spectrum were compared to the results obtained by numerical  
112 simulations. The last fifth section contains a discussion on the eruptive behaviour occurred at Fuego  
113 de Colima during 1998-2018, providing new insights from the observed data and non-linear models.  
114

## 115 **2. The historical activity of Fuego de Colima volcano**

116

117 Since historical times Fuego de Colima represents the most active volcano in Mexico, posing a  
118 serious threat to all surrounding populations (Cortés et al., 2005; Gavilanes-Ruiz et al., 2009;  
119 Bonasia et al., 2011; Roverato et al., 2011). The earliest accounts of the volcano activity can be  
120 found in *Historia Antigua de Mexico* (Clavijero, 1780), where the destructive effects of its  
121 explosive activity are carefully described (Bretón-Gonzales et al., 2002). The historical activity of  
122 Fuego de Colima was described and interpreted by several authors (Luhr and Carmichael, 1980;  
123 Medina-Martínez, 1983; De la Cruz-Reyna, 1993; Bretón-Gonzales et al., 2002; Luhr, 2002). The  
124 Fuego de Colima has shown a transitional eruptive behaviour spanning from effusive to explosive  
125 activity, dominated by dome growth and Vulcanian eruptions. Occasionally sub-Plinian events  
126 occurred (1576, 1606, 1690, 1818 and 1913), indicating a recurrence time of approximately 100  
127 years (De la Cruz-Reyna, 1993; Luhr, 2002; Saucedo et al., 2005; Gavilanes-Ruiz et al., 2009;  
128 Massaro et al. 2018a). The sub-Plinian event occurred in 1913 (Saucedo et al., 2010) is the largest  
129 historical eruption and it has been used as benchmark for volcanic hazard studies (Martin Del Pozzo  
130 et al., 1995; Saucedo et al., 2005; Bonasia et al., 2011).

131

### 132 2.1. The 1998-2018 eruptive activity

133 The 1998-2018 is the only period of post 1913 activity for which there is sufficiently available  
134 information to explore the cyclic activity of Fuego de Colima. Different periods of effusion (domes  
135 and lava flows) punctuated by Vulcanian eruptions and dome collapses characterised the volcano  
136 activity between 1998 and 2018 (Savov et al., 2008; Varley et al., 2010a; Hutchinson et al., 2013;  
137 Mueller et al., 2013; Zobin et al., 2015; GVP, 2017). The duration of extrusive activity and magma  
138 discharge rate varied through time, that was generally divided into five eruptive phases up to 2015;  
139 I) 1998-1999; II) 2001-2003; III) 2004-2005; IV) 2007-2011; V) 2013-2015 (Zobin et al., 2015;  
140 Aràmbula-Mendoza et al., 2018).

141 The first dome extrusion of the 1998-1999 phase started in November 1998, and quickly filled the  
142 1994 explosion crater, forming lava flows that descended the southern flanks of the Fuego de  
143 Colima cone during most of 1999 ( $> 5 \text{ m}^3 \text{ s}^{-1}$  in average for Mueller et al., 2013;  $4.11 \text{ m}^3 \text{ s}^{-1}$  in  
144 average for Reubi et al., 2013).

145 At the beginning, this dome grew rapidly (ca.  $4.4 \text{ m}^3 \text{ s}^{-1}$ ) reaching a volume of ca.  $3.8 \times 10^5 \text{ m}^3$  in  
146 24 hours. During this period the effusion rate reached a peak value around  $30 \text{ m}^3 \text{ s}^{-1}$  (Navarro-  
147 Ochoa et al., 2002; Zobin et al., 2005; Reubi et al., 2015) and showed a cyclic damped behaviour  
148 soon after. During 1999-2001 a series of explosions destroyed the dome and excavated a large  
149 apical crater (Bretòn-Gonzales et al., 2002).

150 A slow outpouring of lava ( $< 1 \text{ m}^3 \text{ s}^{-1}$  for Mueller et al., 2013;  $0.17 \text{ m}^3 \text{ s}^{-1}$  for Reubi et al., 2013;  
151 2015) resumed in May 2001 and continued for 22 months. In February 2002, the lava dome  
152 overflowed the crater rims producing lava flows. During this eruptive phase, the magma extruded  
153 from three separate vents with only minor explosive activity, at a rate of ca.  $0.9 \text{ m}^3 \text{ s}^{-1}$  (GVP, 2002).  
154 Vulcanian explosions dismantled the dome during July and August 2003 (GVP, 2003).

155 In September 2004, low-frequency seismic swarms heralded the onset of the new effusive phase  
156 (Varley et al., 2010a; Arámbula-Mendoza et al., 2011; Lavallée et al., 2012) with a small increase  
157 in average discharge rate of  $0.6 \text{ m}^3 \text{ s}^{-1}$  (Reubi et al., 2013; 2015). The lava dome building occurred  
158 from the end of September until the beginning of November, with a magma effusion rate up to  $7.5$   
159  $\text{m}^3 \text{ s}^{-1}$  in October (Zobin et al., 2008; 2015). The effusive activity was accompanied and followed  
160 by intermittent Vulcanian explosions. The explosive activity diminished in intensity during  
161 December 2004-January 2005. From February to September 2005, effusion and large explosions  
162 occurred.

163 In the following months, small, short-lived domes were observed, with an estimated effusion rate  
164 between  $1.2 - 4.6 \text{ m}^3 \text{ s}^{-1}$  (Varley et al., 2010b; Reubi et al., 2015). In May and June, the explosive  
165 activity produced pyroclastic density currents reaching distances up to 5.4 km from the volcano  
166 summit (Varley et al., 2010a). In February 2007, a new lava dome began to grow and explosions

167 were reported in the period between January 2009 and March 2011. The 2007-2011 period of dome  
168 extrusion represents the slowest growth rate in the recent history of Fuego de Colima. Hutchinson et  
169 al. (2013) calculated a mean effusion rate of ca.  $0.02 \text{ m}^3 \text{ s}^{-1}$  from 2007 to 2010 using digital  
170 photographic data, in good accordance with Zobin et al. (2015) that reported extrusion rates of  $0.03$   
171  $\text{m}^3 \text{ s}^{-1}$  during 2007. Mueller et al. (2013) estimated the magma extrusion rate between  $0.008 \pm 0.003$   
172  $\text{m}^3 \text{ s}^{-1}$  to  $0.02 \pm 0.007 \text{ m}^3 \text{ s}^{-1}$  during 2010, which dropped down to  $0.008 \pm 0.003 \text{ m}^3 \text{ s}^{-1}$  again in  
173 March 2011. On 21 June 2011 an explosion heralded the cessation of dome growth and marked the  
174 end of the effusive period.

175 After 1.5 years of rest, in January 2013 a sequence of explosions cored out the 2011 dome and  
176 generated pyroclastic density currents that reached distances of up to 2.8 km from the summit  
177 (GVP, 2013). From March to October, the calculated discharge rate was in the range of  $0.1 - 0.2 \text{ m}^3$   
178  $\text{s}^{-1}$  (Reyes-Dávila et al., 2016). Successively, the mid-low explosive activity took place up to  
179 February-March 2014, until a new pulse of magma observed in July, with an approximate rate of 1-  
180  $2 \text{ m}^3 \text{ s}^{-1}$  (Aràmbula-Mendoza et al., 2018). On 11 January 2015, a new lava dome was observed  
181 inside the crater (Thiele et al., 2013) and its growth continued until July, with effusion rate of ca.  
182  $0.27 \text{ m}^3 \text{ s}^{-1}$  (Zobin et al., 2015). Between 10-11 July 2015 the recent dome was destroyed by the  
183 most intense activity since the 1913 eruption (Capra et al., 2016; Reyes-Dávila et al., 2016). In the  
184 2013-2015 period, the average extrusion rate was of ca.  $0.2 \text{ m}^3 \text{ s}^{-1}$  (Thiele et al., 2017), with peak  
185 values  $> 10 \text{ m}^3 \text{ s}^{-1}$  (Varley, 2015). After that, the eruptive activity ceased until January 2016 when  
186 daily ash plumes started to occur along with active lava flows and explosions. In early July a new  
187 dome began to grow, overtopping the crater rim. A large explosion was recorded on 10 July 2016,  
188 followed by daily and multiple-daily ash plumes up to the end of year. Multiple flows descended  
189 from lava dome during September-December. In 2017 frequent strong explosions and ash emissions  
190 were recorded until March. Through June decreasing seismicity and minor landslides were reported  
191 with no evidence of effusive activity or new dome growth (GVP, 2017). Here we provide a more  
192 systematic overview of the 1998-2018 erupted activity, obtained by satellite thermal data along with

193 some published data, explained in the following section.

194

### 195 **3. Methods**

196 We analysed the thermal energy spectrum of Fuego de Colima volcano available from March 2000  
197 to October 2018, detected Middle Infrared Observation of Volcanic activity (MIROVA) hot-spot  
198 detection system (Coppola et al., 2016). The period 1998-1999 was integrated using published  
199 discharge rates (Navarro-Ochoa et al., 2002; Zobin et al., 2005). The MIROVA NRT system is  
200 based on the near real time (NRT) analysis of the MODerate resolution Imaging Spectroradiometer  
201 (MODIS) data, distributed by the LANCE-MODIS data [system \(http://modis.gsfc.nasa.gov/\)](http://modis.gsfc.nasa.gov/).

202 The thermal emission from an object is attenuated by the atmosphere resulting from absorption by  
203 gases and scattering by particles. MIROVA system focuses on the Middle InfraRed region (MIR),  
204 which shows the lowest attenuation levels, to better detect and analyse thermal radiation emitted  
205 from volcanic sources. While the standard MODIS forward processing delivers Aqua and Terra  
206 images within 7-8 hours of real time, LANCE-MODIS allows for the creation of MIROVA radiant  
207 flux time series within 1-4 hours from the satellite overpass ([www.mirovaweb.it](http://www.mirovaweb.it)). This thermal data  
208 collection was converted into lava discharge rate estimates and integrated with some published data  
209 in order to reconstruct the weekly mean discharge rate spectrum from 1998 to 2018 (Fig. 2a).

210 In this work, we refer to Coppola et al. (2013), who describes the relationship between the heat lost  
211 by lava thermal radiance variations and discharge rates, by means of a unique, empirical parameter.  
212 They compared the energy radiated during several distinct eruptions to the erupted lava volumes  
213 ( $\text{m}^3$ ). The relationship between the Volcanic Radiated Energy ( $VRE$ ) and the erupted volume was  
214 defined by introducing the concept of radiant density ( $c_{rad}$ , in  $\text{J m}^{-3}$ ). This parameter is analysed as a  
215 function of the  $\text{SiO}_2$  content and the bulk rheological properties of the related lava bodies. It is  
216 strongly controlled by the characteristic thickness of the active lavas at the time of a satellite  
217 overpass, whereas the effects of variable degree of insulation, morphology and topographic



218 conditions produce only a limited range of variability ( $\pm 50\%$ ) (Coppola et al., 2013). For the Fuego  
219 de Colima we used a value of  $c_{rad} = 3.90 \times 10^7 \text{ (J m}^{-3}\text{)}$  for a  $\text{SiO}_2$  content of 59.6% (Savov et al.,  
220 2008; Coppola et al., 2013). We obtained the cumulative volumes of effusion per year (from 2000  
221 to 2018) considering the ratio between the average *VRE* estimations and  $c_{rad}$ . It is important to stress  
222 that the instrumental limit of the MIROVA system is not able to detect thermal anomalies below  
223 0.5–1 MW. Since we used a radiant density ( $c_{rad}$ ) of  $3.90 \times 10^7 \text{ J m}^{-3}$ , the minimum reliable value of  
224 discharge rate is  $0.01 \text{ m}^3 \text{ s}^{-1}$  (Coppola et al., 2013). As reported by Coppola et al. (2016), the  
225 thermal data obtained from MIROVA are not corrected due to the presence/attenuation of clouds.  
226 For this reason, the estimates of effusion rates and volumes are to be considered as minimum  
227 estimates.

228 Because the 2002-2006 and 2013-2016 intervals are the most active in the analysed period, we  
229 firstly applied the Fourier analysis to the monthly average of discharge rates (Fig. 2b) of these time  
230 intervals, in order to explore the modal spectrum of the signal. Although Fourier analysis is well  
231 suited to the quantification of constant periodic components in a time series, it cannot recognise  
232 signals with time-variant frequency content. Whereas a Fourier Transform analysis may determine  
233 all the spectral components embedded in a signal, it does not provide any information about timing  
234 of occurrence. To overcome this problem, several solutions have been developed in the past  
235 decades that are able to represent a signal in the time and frequency domain at the same time.

236 The aim of these approaches is to expand a signal into different waveforms with local time–  
237 frequency properties well adapted to the signal structure (Cazellas et al., 2008). In order to get  
238 information on the amplitude of the periodic signals within the Fuego de Colima (MIROVA) time  
239 series, we performed a wavelet analysis by decomposing the weekly time series (Fig. 2a) into  
240 time/frequency space (Fig. 3).

241 Wavelet analysis is a powerful tool largely used in many scientific fields (i.e., ecology, biology,  
242 climatology, geophysics) and engineering. It is especially relevant to the analysis of non-stationary

243 systems (i.e., systems with short-lived transient components, Cazellas et al., 2008). In particular, the  
244 wavelet analysis is well suited for investigations of the temporal evolution of aperiodic and  
245 transient signals (Lau and Weng, 1995; Mallat, 1998).

246 For this study, practical details in applying wavelet analysis were taken from Torrence and Compo  
247 (1998) and Odbert and Wadge (2009). It is worth noting that wavelet analysis considers a wave  
248 that decays over a finite time and whose integral over infinite time is zero. Many forms of wavelet  
249 (called “wavelet functions”  $\psi(\eta)$ , or “mother functions”, which depend on a non-dimensional time  
250 parameter “ $\eta$ ”) have been designed for analytical use (Farge, 1992; Weng and Lau, 1994;  
251 Daubechies, 1994), each with its own characteristics that make it suitable for certain applications.  
252 The choice of the wavelet can influence the time and scale resolution of the signal decomposition.  
253 Wavelet analysis is popular in geosciences (Trauth, 2006) as it does not require any a priori  
254 understanding of the system generating the time series.

255 Our time series (weakly average discharge rates acquired mainly by the MIROVA system; Fig. 2a),  
256 called  $(x_n)$ , has equal time spacing ( $\delta t = 7$  days) and number of points  $n = 0 \dots N-1$ . Using the  
257 approximately orthogonal Morlet function as wavelet function  $\psi(\eta)$  (it must have zero mean and  
258 be localized in both time and frequency space; Farge, 1992), we here define the wavelet transform  
259  $W_n(s)$  as the convolution of  $x_n$  with a scale ( $s$ ) and translated version of  $\psi_0(\eta)$  (mother function). In  
260 formula:

$$261 \quad W_n(s) = \sum_{n'=0}^{N-1} x_{n'} \psi * \left[ \frac{(n' - n)\delta t}{s} \right] \quad (1)$$

262 where the (\*) indicates the complex conjugate. The scale  $s$  should be equal to approximately  $2\delta t$ ,  
263 according to the Nyquist theorem. Therefore, the smallest wavelet we could possibly resolve is  $2\delta t$ ,  
264 thus we choose  $s_0 = 14$  days. Generally,  $\psi(\eta)$  is a complex function, therefore the wavelet transform  
265 is also complex. It is possible to reconstruct the “local” wavelet power spectrum as the absolute-

266 value squared of the wavelet coefficients,  $|Wn(s)|^2$ . The way to compute the wavelet transform for a  
267 time series is to find the Fourier transform of both the wavelet function (Morlet in our case) and the  
268 time series. Following Torrence and Compo (1998), we made the normalization by dividing by the  
269 square-root of the total wavelet variance ( $\sigma^2$ ).

270 Usually, a periodic component in a time series may be identified in a power spectrum if it has  
271 distinctly greater power than a mean background level (that would correspond to a Gaussian  
272 background noise) (Odbert and Wadge, 2009). However, the spectra generated from many  
273 geophysical systems indicate that the noise in time series data tends not to have a Gaussian  
274 distribution (Vila et al., 2006) but it can be better described by coloured noise, specifically red noise  
275 (Fougere, 1985). For this reason, we use a simple model for red noise given by the univariate lag-1  
276 autoregressive or Markov process (Torrence and Compo, 1998) in order to determine the  
277 significance levels for our wavelet spectrum. These background spectra are used to establish a null  
278 hypothesis for the significance of a peak in the wavelet power spectrum. The null hypothesis is  
279 defined for the wavelet power spectrum considering that the time series has a mean power  
280 spectrum: if a peak in the wavelet power spectrum is significantly above this background spectrum,  
281 then it can be assumed to be a true feature with a certain percentage of confidence. For definitions,  
282 “significant at the 5% level” is equivalent to “the 95% confidence level” (Torrence and Compo,  
283 1998). The confidence interval is defined as the probability that the true wavelet power at a certain  
284 time and scale lies within a certain interval about the estimated wavelet power (Torrence and  
285 Compo, 1998). Because we deal with finite-length time series, errors occur at the beginning and end  
286 of the wavelet power spectrum. A solution is to pad the end of the time series with zeroes to bring  
287 the total length  $N$  up to the next-higher power of two, thus limiting the edge effects. However,  
288 padding with zeroes introduces discontinuities at the endpoints and, especially towards larger  
289 scales, decreasing the amplitude near the edges as more zeroes enter the analysis (Torrence and  
290 Compo, 1998). The cone of influence (COI) is the region of the wavelet spectrum beyond which

291 edge effects become important. The criterion for applying wavelet analysis is very similar to those  
292 employed with classic spectral methods. In other words, the wavelet transform can be regarded as a  
293 generalization of the Fourier transform, and by analogy with spectral approaches, we compute the  
294 local wavelet power spectrum as described above. Successively, this can be compared with the  
295 “global” wavelet power spectrum which is defined as the averaged variance contained in all wavelet  
296 coefficients of the same frequency (Torrence and Compo, 1998; Cazellas et al., 2008).

297 Numerical simulations have been carried out using the magma flow model of Melnik and Costa  
298 (2014), who generalized the model proposed by Melnik and Sparks (2005) and Costa et al. (2007a)  
299 for a magma chamber connected to a dyke that develops into a cylindrical conduit near surface. In  
300 particular, the model of Melnik and Costa (2014) accounts for the possibility of a dual magma  
301 chamber system. The model accounts for rheological changes due to volatile loss and temperature  
302 driven crystallization. These processes are both effective during dome extrusion eruptions because  
303 of the typical low magma ascent velocities (from millimetres to few centimetres per second), which  
304 can result in magma transit times from days to weeks. These ascent times are often comparable with  
305 those of crystal nucleation and growth (Melnik and Sparks, 1999; 2005; Costa et al., 2007c).

306

#### 307 **4. Input and target data for numerical simulations**

##### 308 4.1 Geometrical configurations of the magma plumbing system

309

310 Within the physical framework used in the Melnik and Costa (2014), the model (Fig. 1b) consists of  
311 two elastic magma chambers located at different depths, with chamber pressures  $P_{chs}$  and  $P_{chd}$  able  
312 to drive the magma ascent in elliptical cross-section volcanic conduit (approximating a dyke). Near  
313 surface the conduit develops into a cylinder at depth  $L_T$  (named “transition level”).

314 Numerical simulations were carried out considering the shallower magma chamber (single magma  
315 chamber configuration) or the double magma chamber. The single magma chamber model

316 considers a conduit feeding system composed of a shallow dyke ( $d_s$ ) that connects the magma  
317 chamber to a shallower cylinder, in agreement with geological and geophysical evidence from  
318 different volcanoes (Melnik and Sparks, 2005; Costa et al., 2007a; Melnik et al., 2008; Melnik and  
319 Costa, 2014). The double magma chamber model includes the addition of a deep reservoir  
320 connected to the shallow chamber through a deep elastic dyke ( $d_d$ ) (Fig. 1b).

321 In order to reproduce the observed fluctuations in discharge rates recorded in some periods of the  
322 1998-2018 erupted activity, we considered a discharge rate regime where the period of pulsations is  
323 controlled by the elasticity of the shallow dyke, and a discharge rate regime where the periodicity is  
324 controlled by the volume of the single or dual magma chamber(s) (Barmin et al., 2002; Melnik and  
325 Sparks, 2005; Costa et al., 2007a; Melnik and Costa, 2014).

326 In Appendices A1 and A2 we reported some test simulations in order to show the control of the  
327 most sensitive parameters (i.e. water content in magma, dyke dimensions, volume of magma  
328 chamber, magma influx rate into the magma chamber) affecting the model outputs in case of the  
329 single magma chamber model. The volumes of the magma chamber ( $V_{ch}$ ) range from 20 to 50 km<sup>3</sup>  
330 and the width of the feeder dyke  $2a$  varies from 200 to 400 m (Massaro et al., 2018a).

331 In Appendix A3 is shown the sensitivity test aimed to explore a broad range of chamber volumes  
332 and aspect ratios in the case of double magma chamber configuration. The deep chamber has its top  
333 at 15 km of depth, it is pressurised and fed from below by a constant influx  $Q_{in,d}$ . The volumes of  
334 shallow magma chamber ( $V_{chs}$ ) range from 30 to 50 km<sup>3</sup>, and the volumes of the deep magma  
335 chamber ( $V_{chd}$ ) from 550 to 750 km<sup>3</sup>, according to geophysical data (Cabrera-Espindola, 2010;  
336 Spica et al., 2017). The aspect ratios for shallow and deep magma chambers ( $AR_s - AR_d$ ) varied  
337 from 1 to 2. For each run included in the sections 1-3 of A4, we used a fixed influx  $Q_{in,d}=2.3 \text{ m}^3 \text{ s}^{-1}$ ,  
338 and variable widths of the deeper dyke ( $2a_{od}$ ) from 200 to 3000 m (representative from weak to  
339 strong coupling of the magma chambers; Melnik and Costa, 2014). The lower dyke thickness  $2b_{od}$  is  
340 not an input data of the model as it changes as function of local pressure conditions, therefore it  
341 does not appear in the diagrams. In Section 4 of A3 we show two sets of runs having  $Q_{in,d}$  equal to

342 1 and 3 m<sup>3</sup> s<sup>-1</sup> respectively, and the following fixed parameters:  $AR_s$  and  $AR_d = 1$ ,  $V_{chd} = 650 \text{ km}^3$ ,  
343  $V_{chs} = 40 \text{ km}^3$ .

344

#### 345 4.2 Petrological data

346

347 Erupted products at Fuego de Colima are chemically intermediate and primarily andesitic lavas with  
348 ca. 61 wt.% SiO<sub>2</sub>, (Lavallè et al., 2012). The observed dome growth phases are usually fed by  
349 prolonged magma ascent times, which allow efficient degassing and crystallization. This is in  
350 agreement with the low mean porosity (14-16% e.g Lavallè et al., 2012; Farquharson et al., 2015)  
351 and low water contents of the products of the recent activity (2 wt. % for 1998-1999, Mora et al.,  
352 2002; 0.1-2.5 wt. % for 1998-2005 products, Reubi and Blundy, 2008). Dome lava currently  
353 erupted exhibits a range of crystallinities (phenocrysts, 20–30 vol.%; microlites, 25–50 vol.%), and  
354 the groundmass constitutes as much as 68 vol.% (Luhr, 2002). The andesites show a porphyritic  
355 texture with plagioclase (13–25 vol.%), orthopyroxene (2– 4 vol.%), clinopyroxene (3–4 vol.%) and  
356 minor hornblende (<0.5%) and Fe–Ti oxides (ca. 2 vol.%). Olivine occurs rarely as xenocrysts  
357 (Lavallè et al., 2012).

358 As reported in Melnik and Costa (2014), the magma viscosity  $\mu$  is calculated according to Costa et  
359 al. (2007a) considering the melt viscosity,  $\mu_m$ , times a correction for the effects of crystallinity,  $\theta$ ,  
360 and for the bubbles,  $\eta$ . In formula:

$$361 \mu = \mu_m(c, T) \theta(\beta) \eta(\alpha, Ca) \quad (2)$$

362 which depends on the melt viscosity  $\mu_m$  (that is function of the water content  $c$  and temperature  $T$ ),  
363 on the crystal content  $\beta$ , on bubble fraction  $\alpha$  and on bubble capillarity number  $Ca$ . The rheological  
364 model is described in detail in Costa et al. (2007a). Table 1 summarises the value ranges used for  
365 the input parameters of the model.

## 367 5. Results

368 In Figure 2 we showed the averages of discharge rates at Fuego de Colima volcano from November  
369 1999 to October 2018. Here we define as “high” discharge rates values  $> 0.1 \text{ m}^3 \text{ s}^{-1}$  (highlighted as  
370 dark blue areas). All values below  $0.1 \text{ m}^3 \text{ s}^{-1}$  are considered “low” discharge rates (light blue areas).  
371 Volcanological observations are reported at the top and the bottom of the diagram. It is worth  
372 noting that the “high” and “low” explosive activity correspond to the high and low discharge rate,  
373 respectively. In addition, we distinguished between lava flows and lava domes accordingly to the  
374 dominant emplacement style typical of each eruption, and between “low” (i.e. ash plumes, gas  
375 emissions) and “high” (i.e. strong explosions, Vulcanian eruptions) magnitude explosive activity.

376 The weekly average of discharge rates represents the complete dataset used in this study, and is  
377 reported in Figure 2a. These data have been calculated by using the MIROVA data (black dots) for  
378 the 2000-2018 period, and complemented with published data (blue crosses) for the 1998-1999  
379 period (Navarro-Ochoa et al., 2002; Zobin et al., 2005). Even if the data detection of satellite  
380 thermal energy represents a continuous spectrum of information, it is worth noting that it suffers of  
381 some limitations connected to cloud covering, magma composition, rheology, and emplacement of  
382 the investigated lava body due to topographic conditions (Harris and Rowland, 2009; Harris et al.,  
383 2010; Coppola et al., 2013). Figure 2b shows the monthly discharge rate spectrum from 1998 to  
384 2018 using the MIROVA dataset (black dots), integrated with available published data (blue  
385 crosses) (Navarro-Ochoa et al., 2002; Zobin et al., 2005; Capra et al., 2010; Varley et al., 2010a;  
386 Sulpizio et al., 2010; James and Varley, 2012; Hutchinson et al., 2013; Reubi et al., 2013; Varley,  
387 2015; Reyes-Dávila et al., 2016; Thiele et al., 2017; GVP, 2000; 2017). Figure 2c summarizes the  
388 yearly average of discharge rates from MIROVA dataset, highlighting the good agreement with the  
389 available average estimation of yearly discharge rates from literature (Mueller et al., 2013; Reyes-  
390 Dávila et al., 2016; Aràmbula et al., 2018; GVP, 1998-2017).

391

## 392 5.1 Fourier analysis

393 We applied Fourier analysis to the 1998-2018 dataset (Fig. 2a). In particular, we chose two time  
394 windows: i) 2002-2006 period which showed two periodic components,  $T_0 = 24.70$  and  $T_1 = 6.17$   
395 corresponding to ca. 24 and ca. 6 months, respectively (Appendix A4 Fig. a), and ii) 2013-2016  
396 period that provided similar results:  $T_0 = 24.94$  and  $T_1 = 6.23$  corresponding to ca. 25 and ca. 6  
397 months, respectively (Appendix A4, Fig. b).

398

## 399 5.2 Morlet wavelet analysis

400 The whole analysed dataset is composed of 825 data points, representing the time evolution of the  
401 oscillating components of the 1998-2018 eruptive activity (Fig. 2a). Figure 3a shows the normalised  
402 local wavelet power spectrum of the signal. The colours scale for power values vary from light  
403 orange (low values) to dark red (high values). The thick black contours represent the 95%  
404 confidence level. The blue line indicates the cone of influence (COI) that delimits the region not  
405 influenced by edge effects. From this analysis, it is easy to observe three main periodicities during  
406 2002-2006 and 2013-2016 periods: i) long-term periodicity of ca. 1.5–2.5 years; ii) intermediate-  
407 term periodicity of ca. 5-10 months; and, iii) short-term periodicity of ca. 2.5-5 weeks. The  
408 volcanological observations (about “high” and “low” discharge rates) are also reported in order to  
409 provide a closer link between the observational datasets and the identification of frequency change  
410 in the extrusion rate time series. The short-term periodicity is also present in 2011 (Fig. 3a). Figure  
411 3b shows the global wavelet spectrum corresponding to the local wavelet power spectrum plotted in  
412 Fig. 3a. The green dashed line shows the position of the best-fitting red noise model at the 95%  
413 confidence level.

414



### 415 5.3 Numerical simulations

416 Appendices A1-A3 provide some sensitivity tests in order to explore the effects of different  
417 parameters on discharge rate fluctuations for the single (A1-A2) and dual magma chamber models  
418 (A3). In particular, in Appendix A1 is reported the general steady-state solution of the numerical  
419 model, with both stable and unstable branches (e.g. Melnik et al., 2008; Nakanishi and Koyaguchi,  
420 2008), showing that the cyclic behaviour can occur only between 2 and 4 m<sup>3</sup> s<sup>-1</sup>, for the fixed input  
421 data (panel (a)). Varying the width of the shallow dyke  $2a$  (from 200 to 400 m) and water content in  
422 the melt phase, we observed how the unstable branch changes its shape. This implies different  
423 periods of possible oscillations in discharge rate (panels (b)-(c)).

424 Appendix A2 provides a set of simulations carried out varying the width of the shallow dyke  $2a$   
425 (panel (a)). The resulting periodicities vary from ca. 1000 days ( $2a = 200$  m) ca. 500 days ( $2a = 300$   
426 m) to ca. 250 days ( $2a = 400$  m). These results highlight negative correlation between dyke widths  
427 and periods of oscillation (Costa et al., 2007a). In this case, the variable widths influence the  
428 intensity and periodicity of discharge rates: the wider the dyke, the lower the intensity and  
429 periodicity of discharge rates. Differences in the amplitude of oscillations are observed in panel (b),  
430 highlighting a positive correlation between the volume of the magma chamber  $V_{ch}$  and periodicities.  
431 Periodicities of ca. 500 days correspond to 20 - 30 km<sup>3</sup>, while larger values of ca. 970 and ca. 1176  
432 days are provided for 40 and 50 km<sup>3</sup>, respectively. In panel (c), we reported also a set of simulations  
433 considering the modelled discharge rate controlled by the elasticity of the shallower dyke with fixed  
434 influx rates  $Q_{in}$  (in the range of 0.01 - 0.1 m<sup>3</sup> s<sup>-1</sup>).

435 Appendix A3 contains four sections dedicated to the sensitivity tests for the dual magma chamber  
436 model. As reported in Melnik and Costa (2014), the dual chamber model shows cyclic behaviour  
437 with a period that depends on the intensity of the influx rate and the chamber connectivity  
438 (described as the horizontal extent of the dyke connecting the two chambers). For a weak  
439 connectivity, the overpressure in the deeper chamber remains nearly constant during the cycle and

440 the influx of fresh magma into the shallow chamber is also nearly constant. For a strong  
441 connectivity between the two chambers, their overpressures increase or decrease during the cycle in  
442 a synchronous way. Influx into the shallow chamber stays close to the extrusion rate at the surface  
443 (Melnik and Costa, 2014). We explored different cases considering various fixed parameters as  
444 follow: *i*) volumes of the shallow and deep magma chambers ( $V_{chs} = 40 \text{ km}^3$ ,  $V_{chd} = 650 \text{ km}^3$ ); *ii*)  
445 aspect ratios ( $AR_s = 1$ ,  $AR_d = 1$ ) and the deep magma chamber volume ( $V_{chd} = 650 \text{ km}^3$ ); *iii*) aspect  
446 ratios ( $AR_s = 1$ ,  $AR_d = 1$ ) and the shallow magma chamber volume ( $V_{chs} = 40 \text{ km}^3$ ). For *i*), *ii*) and  
447 *iii*) cases, the deep influx rate  $Q_{in,d}$  has fixed values from 3 to 1  $\text{m}^3/\text{s}$ . In conclusion, these  
448 sensitivity tests showed the passage from weakly connected magma chambers (lack of simultaneous  
449 oscillation of  $Q_{in,s}$  and  $Q_{out}$ ) when  $2a_{0d} = 200 \text{ m}$  to strongly connected magma chambers  
450 (synchronous oscillations of  $Q_{in,s}$  and  $Q_{out}$ ) when  $2a_{0d} = 3000 \text{ m}$ .

451 Figure 4 reported the results of numerical simulations aimed to reproduce the Fuego de Colima  
452 fluctuations during 1998-2018. Figure 4a shows a representative example of time-dependent  
453 solution for a discharge rate controlled by the elasticity of the shallower dyke. Simulations were  
454 carried out using fixed values of pressure (blue line) and influx rate (green line) at the source region  
455 of the shallower dyke, which is ca. 6000 m long. The dyke has width  $2a = 400 \text{ m}$  and thickness  $2b =$   
456  $2 \text{ m}$  and a dyke-cylinder transition  $TL$  at 1300 m of depth. The magma chamber volume is fixed to  
457  $30 \text{ km}^3$ . Solutions present periodicities from 16 to 40 days in agreement with the weekly  
458 periodicities of ca. 38-18 days (ca. 2.5-5 weeks) derived from the wavelet analysis (Fig. 3a).

459 Figure 4b describes a representative example of the single magma chamber model simulations. We  
460 set the magma feeding system composed of a dyke long 6500 m, having a width  $2a = 600 \text{ m}$ ,  
461 thickness  $2b = 4 \text{ m}$ , and a dyke-cylinder transition  $TL$  fixed at 1000 m of depth. The chamber has a  
462 volume fixed to  $30 \text{ km}^3$  and receives a constant  $Q_{in,s} = 2.3 \text{ (m}^3 \text{ s}^{-1})$ . The transient solution is  
463 accounted for the discharge rate controlled by the magma chamber volume, showing an  
464 intermediate-term periodicity of ca. 220 days, in agreement with the intermediate-term periodicity  
465 of ca. 146-292 days (ca. 5-10 months) obtained from the wavelet analysis (Fig. 3a).

466 Figure 4c reports a representative example of the solution obtained with the dual magma chamber  
467 model in order to assess the effect of the deep chamber on the discharge rate. We fixed the volumes  
468 of deep and shallow magma chamber at 40 and 650 km<sup>3</sup>, respectively. The shallow dyke is 6500 m  
469 long with a width  $2a = 260$  m and thickness  $2b = 4$  m. The deep dyke has a width  $2a_{od} = 500$  m and  
470 a deep influx rate  $Q_{in,d} = 2.3$  (m<sup>3</sup> s<sup>-1</sup>). A cyclic behaviour of ca. 825 days is observed, reaching a  
471 peak discharge rate of ca. 6 (m<sup>3</sup> s<sup>-1</sup>). This result is in agreement with the long-term periodicity of ca.  
472 547-913 days (ca. 1.5 - 2.5 years) derived from the wavelet analysis (Fig. 3a).

473 Considering uncertainties in both modelling results and parameters and the fact that the thickness  
474 and width of the dykes are function of the local overpressure, results are quite consistent, although  
475 with a single model configuration the current approach cannot reproduce at the same time the  
476 periodicity observed at different time scales.

477

478

## 479 **6. Discussions**

480

481 In recent years, many studies have focused on magma flow dynamics in volcanic conduits during  
482 lava dome building eruptions (Melnik and Sparks, 1999; Wylie et al., 1999; Barmin et al., 2002;  
483 Melnik and Sparks, 2002; 2005; Costa et al., 2007a,b; Nakanishi and Koyaguchi, 2008; Kozono and  
484 Koyaguchi, 2012), highlighting periodic variations in discharge rate due to the transition from low  
485 regime (allowing efficient crystals growth leading to an increase in magma viscosity) to high  
486 regime (with negligible crystallization). This difference in discharge rates can be of orders of  
487 magnitude, with strongly non-linear responses to the variation of governing parameters from the  
488 volcanic system. This behaviour allows periodic oscillations of the discharge rate (Nakada et al.,  
489 1999; Watts et al., 2002), as observed in different dome extrusion eruptions (e.g. Mt St. Helens,  
490 Santiaguito, Soufrière Hills; Melnik et al., 2008). Although each volcano usually shows its complex  
491 pattern of discharge fluctuations, the cause can be explained as the superimposition of long,

492 intermediate, and short-term effects of the coupled magma chamber(s) and conduit dynamics. The  
493 long-term oscillations in discharge rate are function of magma chamber size, magma  
494 compressibility, amount and frequency of magma recharge and withdrawal (Barmin et al., 2002;  
495 Costa et al., 2007b; Melnik et al., 2008; Costa et al., 2013). The short-term and intermediate  
496 oscillation dynamics can also superimpose to the main long-term periodicity, through small changes  
497 in magma temperature, water content, and kinetic of crystallization during magma transit in the  
498 conduit (e.g., Melnik et al., 2008). The aforementioned eruptive behaviour characterized also the  
499 Fuego de Colima activity in the 1998-2018 period, as demonstrated by the wavelet analysis of  
500 satellite thermal data. It is important to stress that the oscillating behaviour is not regular, having a  
501 period, between 2007 and 2012, that does not show any significant periodicity (Fig. 3a), possibly  
502 indicating a damped oscillation (Appendix A2). During this period the volcano enter in an almost  
503 quiescent status with very low discharge rates. This period of low discharge rates is punctuated by  
504 low explosive activity, triggered by dome collapse or pressurization of the upper conduit.

505 It is well known for Fuego de Colima that Vulcanian explosions can evacuate significant portions of  
506 the upper conduit and destroy the lava dome. The influence of these processes on the periodicity of  
507 at least short-term periodic regimes could be significant. However, it is expected that such  
508 processes should affect mainly sub-daily periodicities, as explained by Costa et al. (2012) who  
509 analysed the periodicity variations due to the collapse of 200 m high plug at Montserrat. These  
510 changes should also have significant effects on the multi-week periodicity analysed here. Certainly,  
511 it is not excluded that an exceptional large evacuation of the upper conduit would be able to  
512 influence longer periodicities as those investigated here, causing a transition to a more explosive  
513 eruptive style (i.e. Plinian) (Massaro et al., 2018a).

514 In order to investigate the relationship between the periodic components observed in wavelet  
515 analysis and the dynamics of the Fuego de Colima feeding system, we run simulations using the  
516 numerical model Melnik and Costa (2014) (Fig. 4). The model can reproduce the results of the  
517 wavelet analysis in terms of observed periodicities, allows us to relate short-, intermediate- and

518 long-term oscillations in discharge rates to the dynamics of upper conduit, shallow magma  
519 chamber, and coupled shallow and deep magma chambers, respectively. This implies that the  
520 pressurization of the deep magma chamber has cascade effects on the whole feeding system of the  
521 Fuego the Colima, similarly to what observed in other recent lava dome eruptions (i.e. Montserrat;  
522 (Melnik and Costa, 2014). It is of particular interest that the best output with the dual magma  
523 chamber model indicates that chambers do not oscillate simultaneously (“decoupled oscillation”;  
524 Fig. 4c). Although the presented data provide, for the first time, a framework able to describe the  
525 periodic behaviour of effusive activity at Fuego de Colima volcano, both numerical model and  
526 wavelet analysis suffer of some limitations that need to be taken into account in interpreting the  
527 results:

528 *i)* the available data of discharge rates and dome volumes collected for the 1998-2018  
529 period do not have the same quality. For this reason, this lead us to extract only averages of  
530 discharge rate for the entire period, with biasing effects to lower amplitudes;

531 *ii)* a common weakness of the spectral and wavelet analysis techniques is their inability to  
532 distinguish the source of any given periodic component (i.e. whether it is a signal from a  
533 volcanic process, an external process or if it is noise in the dataset). Elucidating the exact  
534 mechanism requires competing robust models and multiple independent field observations  
535 (Odbert and Wadge, 2009);

536 *iii)* assumptions behind the numerical model imply several limitations, such as those due to  
537 the constant value of the dyke width and simplified Newtonian rheology. The first  
538 assumption greatly oversimplifies the physics. In the case of large overpressures, stress at  
539 the dyke tips will exceed the fracture toughness of the rocks and the dyke will expand  
540 horizontally (Massaro et al., 2018b), reaching some equilibrium configuration. When the  
541 deep chamber deflates, overpressure in the deeper dyke will decrease and, as flow rate  
542 decreases, magma at the dyke tips can solidify, leading to a decrease in  $2a_{0d}$  (Kavanagh and  
543 Sparks, 2011; Melnik and Costa, 2014). Thermal exchange with wall rock can also affect

544 the nonlinear dynamics of the system (Costa and Macedonio, 2002; Melnik et al., 2008). In  
545 addition, a more realistic estimate of the magma viscosity during lava dome eruptions  
546 should account for the coupling with energy loss, viscous dissipation, and stick–slip effects  
547 (e.g. Costa and Macedonio, 2005; Costa et al. 2007c; 2013).

548 Although this study revealed that different periodic signals are controlled by different mechanisms  
549 occurring in the plumbing system, the current model approach is not able describe the three  
550 periodicities (long-, intermediate- and short-term) using a unique model configuration.  
551 Nevertheless, we hope this work will motivate further numerical modelling approaches in order to  
552 develop more sophisticated models able to describe the three time scales together, by incorporating  
553 further physical aspects (e.g. full thermal effects) and considering fully 3D geometries.

554

555

## 556 **7. Conclusions**

557

558 The coupling of wavelet analysis and numerical modelling allowed to decipher the eruptive  
559 behaviour of Fuego de Colima in the period 1998-2018, as revealed by satellite thermal data. Three  
560 periodicities emerged from the study: i) long-term ii) intermediate-term, and, iii) short-term.

561 The long-term periodicity extracted from wavelet analysis is ca. 913-547 days (ca. 1.5-2.5 years). It  
562 was replicated by the dual magma chamber model which provided a periodicity of ca. 1000-500  
563 days. The intermediate-term periodicity obtained from wavelet analysis is ca. 146-292 days (ca. 5-  
564 10 months), fairly replicated by the single magma chamber model with a periodicity of ca. 220  
565 days. The short-term periodicity of ca. 18-38 days (ca. 2.5-5 weeks) is matched by model outputs  
566 considering the dynamics of the upper conduit (ca. 16-40 days). The depicted behaviour of effusive  
567 activity at Fuego de Colima is here presented for the first time, showing how the volcano presents

568 similarities with eruptive dynamics of other recent lava dome eruptions (i.e. SHV, Montserrat,  
569 Costa et al., 2013).

570

571

### 572 **Code availability**

573 Melnik and Costa (2014) code is a research software and is not still available for distribution as it  
574 lacks of documentation. It can be used by contacting the authors under their supervision.

575

576

### 577 **Data availability**

578 The original thermal dataset is available on [www.mirovaweb.it](http://www.mirovaweb.it). Excel worksheets can be obtained  
579 by contacting the authors.

580

581

582

## 583 **Appendices**

584

585 **Appendix A1.** Sensitivity tests for steady state solutions of discharge rate vs chamber pressure (top)  
586 and time evolution of discharge rates (bottom). These solutions are referred to the following main  
587 input parameters: i) dyke thickness  $2b = 40$  m as the conduit diameter at the top ( $D=2b$ ), the  
588 transition from the dyke to cylindrical conduit  $L_T = 500$  m below the surface, the length of the dyke  
589  $L_d = 6$  km, and the volume of the magma chamber  $V_{ch} = 50$  km<sup>3</sup>. (a) General solution showing the  
590 transient regime where the periodicity can occur; (b) Solutions influenced by the dyke width  $2a$   
591 (from 200 to 400 m); (c) Solutions influenced by the proportion of the water content in the melt  
592 (H<sub>2</sub>O from 4 to 5 %).

593

594 **Appendix A2.** Sensitivity tests for transient solutions using the single magma chamber model. As a  
595 reference these solutions have the same main input parameters used for A1. (a) Dependence of  
596 discharge rate on time considering the influence of the dyke width  $2a$  (from 200 to 400 m); (b)  
597 Influence of the magma chamber volume  $V_{ch}$  (from 20 to 50 km<sup>3</sup>); (c) Dependence of discharge rate  
598 on time considering the dyke elasticity. Each curve shows a solution with a constant influx rate  $Q_{in}$   
599 (in the range of 0.01- 0.1 m<sup>3</sup> s<sup>-1</sup>).

600

601 **Appendix A3.** Sensitivity tests for transient solutions using the dual magma chamber model. The  
602 shallow feeding system has dyke with a width  $2a = 200$  m,  $2b = 40$  m, and  $L_T = 500$  m. The  
603 cylindrical conduit diameter  $D = 2b$ . For each diagram, is indicated the outflow ( $Q_{out}$ ; black red and  
604 green lines), the flux entering into the shallower magma chamber ( $Q_{ins}$ ; blue line) and periods in  
605 days (T). Runs of Section 1-2-3 have fixed  $Q_{in,d} = 2.3$  (m<sup>3</sup> s<sup>-1</sup>).

- 606 • *Section 1)* The volumes of the shallow and deep magma chambers are fixed to  $40 \text{ km}^3$  and  
607  $650 \text{ km}^3$ , respectively. A set of runs is carried out for three different aspect ratios ( $AR$ ) of the  
608 shallow and deep chambers ( $AR_s = 1$ ;  $AR_d = 1$ ,  $AR_s = 2$ ;  $AR_d = 1$ ,  $AR_s = 2$ ;  $AR_d = 1.5$ )  
609 considering three widths of the deeper dyke ( $2a_{od} = 200 \text{ m}$  - black line,  $1000 \text{ m}$  - red line,  
610  $3000 \text{ m}$  - green line).
- 611 • *Section 2)* The volume of the deeper magma chamber and the aspect ratios of both shallow  
612 and deep chambers are fixed to  $650 \text{ km}^3$  and  $AR_s = AR_d = 1$ . A set of runs is provided for  
613 three different shallow chamber volumes ( $V_{chs} = 30 \text{ km}^3$ ,  $40 \text{ km}^3$ ,  $50 \text{ km}^3$ ) considering three  
614 widths of the deeper dyke ( $2a_{od} = 200 \text{ m}$  - black line,  $1000 \text{ m}$  - red line,  $3000 \text{ m}$  - green  
615 line);
- 616 • *Section 3)* The shallow chamber volume and the aspect ratios of both shallow and deep  
617 chambers are fixed to  $40 \text{ km}^3$  and  $AR_s = AR_d = 1$ , respectively. A set of runs is carried out  
618 for three deep chamber volumes ( $V_{chd} = 550 \text{ km}^3$ ,  $650 \text{ km}^3$ ,  $750 \text{ km}^3$ ) considering three  
619 widths of the deeper dyke ( $2a_{od} = 200 \text{ m}$  - black line,  $1000 \text{ m}$  - red line,  $3000 \text{ m}$  - green  
620 line).
- 621 • *Section 4)* The shallow and deep chamber volumes are fixed to  $40 \text{ km}^3$  and  $650 \text{ km}^3$ ,  
622 respectively. Two set of runs are carried out for  $Q_{in,d}$  equal to 1 and 3 ( $\text{m}^3 \text{ s}^{-1}$ ). The aspect  
623 ratios ( $AR$ ) of the shallow and deep chambers are both equal to 1, considering three widths  
624 of the deeper dyke ( $2a_{od} = 200 \text{ m}$  - black line,  $1000 \text{ m}$  - red line,  $3000 \text{ m}$  - green line).

625  
626  
627 **Appendix A4.** Results of the Fourier analysis. (a) The 2002-2006 period shows two main periodic  
628 components,  $T_0 = 24.70$  and  $T_1 = 6.17$  months, corresponding to ca. 2 years and ca. 6 months,  
629 respectively; (b) The 2013-2016 period shows similar results:  $T_0 = 24.94$  and  $T_1 = 6.23$  months,  
630 corresponding to ca. 2.1 years and ca. 6 months, respectively.

631  
632  
633 **Author's contribution**

634  
635 SM and AC compiled the numerical simulations and formulated the adopted methodology. DC  
636 provided and processed the satellite thermal data. LC provided the volcanological data. SM and RS  
637 wrote the manuscript with the input of all co-authors. All authors worked on the interpretation of  
638 the results.

639  
640  
641 **Competing interests**

642 The authors declare that they have no conflict of interest.



643 **Acknowledgments**

644  
645 SM thanks Centro de Geociencias of Queretaro (UNAM, Mexico) for the hospitality during the  
646 period of research at Fuego de Colima volcano, the Doctoral Course in Geoscience of University of  
647 Bari (Italy) for the partial financial support, and Dr. F. Loparco for the help with the Python coding.  
648 LC was supported by PAPIIT-UNAM n° 105116 project. All authors are grateful to the reviewers  
649 for their valuable comments and suggestions useful to improve the manuscript.  
650

651

652 **References**

- 653  
654 Aràmbula-Mendoza, R., Lesage, P., Valdèz-Gonzales, C., Varley, N., Reyes-Dàvila, G. and  
655 Navarro-Ochoa, C.: Seismic activity that accompanied the effusive and explosive eruptions  
656 during the 2004–2005 period at Volcàn de Colima, Mexico, *J. Volcanol. Geotherm. Res.*,  
657 205, 30–46, 2011.
- 658 Aràmbula-Mendoza, R., Reyes-Dàvila, G., Dulce, M. V. B., González-Amezcuca, M., Navarro-  
659 Ochoa, C., Martínez-Fierros, A., and Ramírez-Vázquez, A.: Seismic monitoring of  
660 effusive-explosive activity and large lava dome collapses during 2013–2015 at Volcàn de  
661 Colima, Mexico. *J. Volcanol. Geotherm. Res.*, 351, 75-88, 2018.  
662
- 663 Barmin, A., Melnik, O. and Sparks, R.S.J.: Periodic behavior in lava dome eruptions, *Earth*  
664 *Planet. Sci. Lett.*, 199 (1), 173-184, 2002.  
665
- 666 Belousov, A., Voight, B., Belousova, M. and Petukhin, A.: Pyroclastic surges and flows from the 8-  
667 10 May 1997 explosive eruption of Bezymianny volcano, Kamchatka, Russia, *B. Volcanol.*,  
668 64 (7), 455-471, 2002.  
669
- 670 Bernstein, M., Pavez, A., Varley, N., Whelley, P. and Calder, E.S.: Rhyolite lava dome growth  
671 styles at Chaitén Volcano, Chile (2008-2009): Interpretation of thermal imagery, *Andean*  
672 *Geology*, 40 (2), 2013.  
673
- 674 Brèton-Gonzalez, M., Ramirez, J.J. and Navarro-Ochoa, C.: Summary of the historical eruptive  
675 activity of Volcan de Colima, Mexico 1519-2000, *J. Volcanol. Geotherm. Res.*, 117, 21–46,  
676 2002.  
677
- 678 Bonasia, R., Capra, L., Costa, A., Macedonio, G., and Saucedo, R.: Tephra fallout hazard  
679 assessment for a Plinian eruption scenario at Volcàn de Colima (Mexico), *J. Volcanol.*  
680 *Geotherm. Res.*, 203, 12-22, 2011.  
681
- 682 Capra, L., Borselli, L., Varley, N., Gavilanes-Ruiz, J. C., Norini, G., Sarocchi, D., and Cortes, A.:  
683 Rainfall-triggered lahars at Volcàn de Colima, Mexico: surface hydro-repellency as  
684 initiation process. *J. Volcanol. Geotherm. Res.*, 189 (1-2), 105-117, 2010.  
685
- 686 Capra, L., Macías, J.L., Cortés, A., Dàvila, N., Saucedo, R., Osorio-Ocampo, S., Arce, J.L.,  
687 Galvilanes-Ruiz, J.C., Corona-Càvez, P., Gàrcia-Sancez, L., Sosa-Ceballos, G., Vasquez, R.:  
688 Preliminary report on the July 10–11, 2015 eruption at Volcàn de Colima: Pyroclastic  
689 density currents with exceptional runouts and volume, *J. Volcanol. Geotherm. Res.*, 310,

- 690 39-49, 2016.
- 691 Cazelles, B., Chavez, M., Berteaux, D., Ménard, F., Vik, J. O., Jenouvrier, S., and Stenseth, N.C.:  
692 Wavelet analysis of ecological time series. *Oecologia*, 156(2), 287-304, 2008.
- 693
- 694 Christopher, T.E., Blundy, J., Cashman, K., Cole, P., Edmonds, M., Smith, P. J., and Stinton, A.:  
695 Crustal-scale degassing due to magma system destabilization and magma-gas decoupling  
696 at Soufrière Hills Volcano, Montserrat. *Geochem. Geophys. Geosyst.*, 16(9), 2797-2811,  
697 2015.
- 698 Coppola, D., Piscopo, D., Staudacher, T. and Cigolini, C.: Lava discharge rate and effusive  
699 pattern at Piton de la Fournaise from MODIS data. *J. Volcanol. Geotherm. Res.*, 184 (1–2),  
700 174–192, 2009.
- 701 Coppola, D., Laiolo, M., Piscopo, D. and Cigolini, C.: Rheological control on the radiant  
702 density of active lava flows and domes. *J. Volcanol. Geotherm. Res.*, 249, 39-48, 2013.
- 703
- 704 Coppola, D., Laiolo, M., Cigolini, C., Delle Donne, D., and Ripepe, M.: Enhanced volcanic hot-  
705 spot detection using MODIS IR data: results from the MIROVA system. *Geol. Soc.*  
706 *London, Special Publications*, 426(1), 181-205, 2016.
- 707
- 708 Costa A. and Macedonio G.: Nonlinear phenomena in fluids with temperature-dependent viscosity:  
709 a hysteresis model for magma flow in conduits, *Geophys. Res. Lett.*, 29, 1402, 2002.
- 710
- 711 Costa A. and Macedonio, G: Viscous heating in fluids with temperature-dependent viscosity:  
712 Triggering of secondary flows, *J. Fluid Mech.*, 540, 21– 38, 2005.
- 713
- 714 Costa, A., Melnik, O., Sparks, R.S.J.: Controls of conduit geometry and wallrock elasticity on lava  
715 dome eruptions, *Earth Planet. Sci. Lett.*, 260, 137–151, 2007a.
- 716
- 717 Costa, A., Melnik, O., Sparks R.S.J. and Voight, B.: Control of magma flow in dykes on  
718 cyclic lava dome extrusion, *Geophys. Res. Lett.*, 34 (2), 2007b.
- 719
- 720 Costa, A., Melnik, O. and Vedeneeva, E.: Thermal effects during magma ascent in conduits, *J.*  
721 *Geophys. Res.*, Vol. 112, B12205, 2007c.
- 722
- 723 Costa A., Caricchi L., Bagdassarov N.: A model for the rheology of particle-bearing  
724 suspensions and partially molten rocks, *Geochem. Geophys. Geosyst.*, 10, Q03010,  
725 doi:10.1029/2008GC002138, 2009.
- 726
- 727 Costa, A., Wadge, G., Melnik, O.: Cyclic extrusion of a lava dome based on a stick-slip  
728 mechanism. *Earth Planet. Sci. Lett.*, 337, 39-46, 2012.
- 729
- 730 Costa, A., Wadge, G., Stewart, R., Odbert, H.: Coupled subdaily and multiweek cycles during the  
731 lava dome eruption of Soufrière Hills Volcano, Montserrat. *J. Geophys. Res., Solid Earth*,  
732 118(5), 1895-1903, 2013.
- 733
- 734 Clavijero, F.X.: *Historia Antigua de Mexico*, Sepan Cuantos, 29, Porrúa, 1780.
- 735
- 736 Cortés, A., Garduño-Monroy, V.H., Navarro-Ochoa, C., Komorowski, J.C., Saucedo, R., Macías,  
737 J.L. and Gavilanes, J.C.: *Carta geológica del Complejo Volcánico de Colima*, con

- 738 Geología del Complejo Volcánico de Colima, Univer. Nat. Autón. México, Inst. Geol.,  
739 Cartas Geológicas y Mineras, 10, 2005.
- 740 Daubechies: Ten Lectures on Wavelets. Society for Industrial and Applied Mathematics, 357, 1992.
- 741 De Bélizal, É., Lavigne, J.C., Gaillard, D. Grancher, I. Pratomio, I., and Komorowski, J.C.: The  
742 2007 eruption of Kelut volcano (East Java, Indonesia): phenomenology, crisis  
743 management and social response, *Geomorphology*, 136(1), 165-175, 2012.  
744
- 745 De la Cruz-Reyna, S.: Random patterns of activity of Colima Volcano, Mexico, *J. Volcanol.*  
746 *Geotherm. Res.*, 55, 51–68, 1993.  
747
- 748 Denlinger, R.P. and Hoblitt, R.P.: Cyclic eruptive behavior of silicic volcanoes, *Geology*, 27 (5),  
749 459-462 1999.  
750
- 751 Dragoni, M. and Tallarico, A.: Assumption in the evaluation of lava effusion rates from heat  
752 radiation. *Geoph. Res. Lett.*, 36, L08302, 2009.
- 753 Farge, M.: Wavelet transforms and their applications to turbulence. *Annu. Rev. Fluid Mech.*, 24,  
754 395–457, 1992.
- 755 Farquharson, J., Heap, M.J., Varley, N. R., Baud, P. and Reuschlé, T.: Permeability and porosity  
756 relationships of edifice-forming andesites: a combined field and laboratory study. *J. Volcanol.*  
757 *Geotherm. Res.*, 297, 52-68, 2015.  
758
- 759 Fougere, P.: On the accuracy of spectrum analysis of red noise processes using maximum entropy  
760 and periodogram models: simulation studies and application to geophysical data. *J.*  
761 *Geophys. Res.* 90, 4355–4366, 1985.
- 762
- 763 Garel, F., Kaminski, E., Tait, S., Limare, A.: An experimental study of the surface thermal  
764 signature of hot subaerial isoviscous gravity currents: implications for thermal monitoring of  
765 lava flows and domes. *J. Volcanol. Geotherm. Res.*, 117, B02205, 2012.
- 766 Gavilanes-Ruiz, J.C., Cuevas-Muñiz, A., Varley, N., Gwynne, G., Stevenson, J., Saucedo-Girón,  
767 R., and Cortés-Cortés, A.: Exploring the factors that influence the perception of risk: The  
768 case of Volcán de Colima, Mexico, *J. Volcanol. Geotherm. Res.*, 186(3), 238-252, 2009.  
769
- 770 Global Volcanism Program: Report on Colima (Mexico). In: Wunderman, R (ed.), *B. Global*  
771 *Volcanism Net.*, 23-10, Smithsonian Institution, 1998.  
772
- 773 Global Volcanism Program: Report on Colima (Mexico). In: Wunderman, R (ed.), *Bulletin of the*  
774 *Global Volcanism Network*, 25-6, Smithsonian Institution, 2000.  
775
- 776 Global Volcanism Program: Report on Colima (Mexico). In: Wunderman, R (ed.), *B. Global*  
777 *Volcanism Net.*, 27-11, Smithsonian Institution, 2002.  
778
- 779 Global Volcanism Program: Report on Colima (Mexico). In: Venzke, E (ed.), *B. Global*  
780 *Volcanism Net.*, 28-11, Smithsonian Institution, 2003.  
781
- 782 Global Volcanism Program: Report on Colima (Mexico). In: Wunderman, R (ed.), *B. Global*  
783 *Volcanism Net.*, 38-12, Smithsonian Institution, 2013.

784  
785 Global Volcanism Program: Report on Colima (Mexico). In: Sennert, S K (ed.), Weekly Volcanic  
786 Activity Report, 26 July-1 August 2017, Smithsonian Institution and US Geological Survey,  
787 2017.  
788

789 Harris, A.J., Rose, W.I. and Flynn, L.P.: Temporal trends in lava dome extrusion at Santiaguito  
790 1922-2000, *B. Volcanol.*, 65(2), 77-89, 2003.  
791

792 Harris, A.J.L., Rowland, S.K.: Effusion rate controls on lava flow length and the role of heat  
793 loss: a review. In: Thordarson, T., Self, S., Larsen, G., Rowland, S.K., Hoskuldsson, A.  
794 (Eds.), *Studies in Volcanology: The Legacy of George Walker: Special Publication*  
795 *IAVCEI*, 2, pp. 33–51, 2009.

796 Harris, A.J.L., Favalli, M., Steffke, A., Fornaciai, A., Boschi, E.: A relation between lava  
797 discharge rate, thermal insulation, and flow area set using lidar data. *Geoph. Res.*  
798 *Lett.*, 37, L20308. <http://dx.doi.org/10.1029/2010GL044683>, 2010.

799 Heap, M.J., Lavallée, Y., Petrakova, L., Baud, P., Reuschle, T., Varley, N., and Dingwell D.B.:  
800 Microstructural controls on the physical and mechanical properties of edifice-forming  
801 andesites at Volcán de Colima, Mexico, *Solid Earth*, 119 (4), 2925-2963, 2014.  
802

803 Hutchison, W., Varley, N., Pyle, D.M., Mather, T.A., and Stevenson, J.A.: Airborne thermal  
804 remote sensing of the Volcán de Colima (Mexico) lava dome from 2007 to 2010, *Geol. Soc.*  
805 *London, Spec. Public.*, 380 (1), 203-228, 2013.  
806

807 James, M. R. and Varley, N.: Identification of structural controls in an active lava dome with high  
808 resolution DEMs: Volcán de Colima, Mexico. *Geoph. Res.Lett.*, 39(22), 2012.  
809

810 Kavanagh, J. L. and Sparks, R.S.J.: Insights of dyke emplacement mechanics from detailed 3D dyke  
811 thickness datasets. *J.Geol. Soc.*, 168(4), 965-978, 2011.  
812

813 Kozono, T. and Koyaguchi, T.: Effects of relative motion between gas and liquid on 1-dimensional  
814 steady flow in silicic volcanic conduits: 2. Origin of diversity of eruption styles. *J.*  
815 *Volcanol. Geotherm. Res.*, 180(1), 37-49, 2009.  
816

817 Kozono, T. and Koyaguchi, T.: Effects of gas escape and crystallization on the complexity of  
818 conduit flow dynamics during lava dome eruptions. *Geoph. Res.Lett.*, *Solid Earth*, 117(B8),  
819 2012.  
820

821 Lamb, O.D., Varley, N., Mather, T.A., Pyle, D.M., Smith, P.J. and Liu, E.J.: Multiple timescales of  
822 cyclical behaviour observed at two dome-forming eruptions, *J. Volcanol. Geotherm. Res.*,  
823 284, 106-121, 2014.  
824

825 Lau K.M. and Weng H.: Climatic signal detection using wavelet transform: how to make a time  
826 series sing. *Bull Am Meteorol Soc.*, 76. 2391–2402, 1995.

827 Lavallée, Y., Varley, N., Alatorre-Ibargüengoitia, M.A., Hess, K.U., Kueppers, U., Mueller, S.,  
828 Richard, D., Scheu, B., Spieler, O. and D.B. Dingwell, D.B.: Magmatic architecture of  
829 dome-building eruptions at Volcan de Colima (Mexico), *Bull. Volcanol.*, 74 (1), 249-260,  
830 2012.  
831

- 832 Lensky, N.G., Navon, O. and Lyakhovsky, V.: Bubble growth during decompression of magma:  
833 experimental and theoretical investigation, *J. Volcanol. Geotherm. Res.*, 129 (1), 7-22, 2004.  
834
- 835 Loughlin, S.C., Luckett, R., Ryan, G., Christopher, T., Hards, V., De Angelis, S. and Strutt, M.: An  
836 overview of lava dome evolution, dome collapse and cyclicity at Soufrière Hills Volcano,  
837 Montserrat, 2005–2007, *Geophys. Res. Lett.*, 37 (19), 2010.  
838
- 839 Luhr, J.F. and Carmichael, I.S.: The Colima Volcanic Complex, Mexico, *Con.to Mineral.Petrol.*, 71  
840 (4), 343-372, 1980.  
841
- 842 Luhr, J.F.: Petrology and geochemistry of the 1991 and 1998-1999 lava flows from Volcan  
843 Colima, Mexico, *J. Volcanol. Geotherm. Res.*, 117, 169–194, 2002.  
844
- 845 Macias, J., Arce, J., Sosa, G., Gardner, J.E., Saucedo, R.: Storage conditions and magma  
846 processes triggering the 1818CE Plinian eruption of Volcán de Colima, *J. Volcanol.  
847 Geotherm. Res.*, doi:10.1016/j.jvolgeores.2017.02.025, 2017.
- 848 Mallat, S.: *A wavelet tour of signal processing*. Academic Press, San Diego, 1998.
- 849 Massaro, S., Sulpizio, R., Costa, A., Capra, L., Lucchi, F.: Understanding eruptive style variations  
850 at calc-alkaline volcanoes: the 1913 eruption of Fuego de Colima volcano (Mexico), *B.  
851 Volcanol.*, 80-62, <https://doi.org/10.1007/s00445-018-1235-z>, 2018a.
- 852 Massaro, S., Costa, A., Sulpizio, R.: Time evolution of a magma feeding system during a Plinian  
853 eruption: the example of the Pomici di Avellino eruption of Somma-Vesuvius (Italy), *Earth  
854 Planet. Sci. Lett.* 482, 545-555, 2018b.  
855
- 856 Medina-Martinez, F.: Analysis of the eruptive history of the Volcán de Colima, Mexico (1560–  
857 1980), *Geofisica Internacional*, 22, 157–178, 1983.  
858
- 859 Martin del Pozzo, A.L., Sheridan, M., Barrera, D., Lugo Hubp, J. and Vázquez Selem, L.:  
860 Potential hazards from Colima volcano, Mexico, *Geofisica Internacional*, 34 (4), 363-376.  
861 1995.  
862
- 863 Melnik, O. and Sparks, R.S.J.: Nonlinear dynamics of lava dome extrusion, *Nature*, 402  
864 (6757), 37-41, 1999.  
865
- 866 Melnik, O. and Sparks, R.S.J: Dynamics of magma ascent and lava extrusion at Soufrière  
867 Hills Volcano, Montserrat, *Geol. Soc. London Mem.*, 21 (1), 153-171, 2002.  
868
- 869 Melnik, O. and Sparks, R.S.J: Controls on conduit magma flow dynamics during lava-dome  
870 building eruptions, *J. Geophys. Res.*, 110, B02209, doi:10.1029/2004JB003183, 2005.
- 871 Melnik, O., Sparks, R.S.J., Costa, A. and Barmin, A.: (2008), *Volcanic Eruptions: Cyclicity during  
872 Lava Dome Growth*, in Meyers: *Encyclopedia of Complexity and Systems Science*, 2008.  
873
- 874 Melnik, O. and A. Costa, A: Dual-chamber-conduit models of non-linear dynamics behaviour at  
875 Soufrière Hills Volcano, Montserrat, *Geol. Soc. Lond., Mem.*, 39, 61-69, 2014.  
876

- 877 Mériaux, C. and Jaupart, C: Simple fluid dynamic models of volcanic rift zones, *Earth Planet. Sci.*  
878 *Lett.*, 136(3-4), 223-240, 1995.
- 879
- 880 Mora, J. C., Macias, J. L., Saucedo, R., Orlando, A., Manetti, P., and Vaselli, O.: Petrology of the  
881 1998–2000 products of Volcán de Colima, México. *J. Volcanol. Geotherm. Res.*, 117(1),  
882 195-212, 2002.
- 883
- 884 Mueller, S.B., Varley, N., Kueppers, U., Lesage, P. and Reyes-Dávila, G.: Quantification of  
885 magma ascent rate through rockfall monitoring at the growing/collapsing lava dome of  
886 Volcan de Colima, Mexico, *Solid Earth*, 4, 201-213, 2013.
- 887
- 888 Nakanishi, M. and Koyaguchi, T.: A stability analysis of a conduit flow model for lava dome  
889 eruptions. *J. Volcanol. Geotherm. Res.*, 178(1), 46-57, 2008.
- 890
- 891 Nakada, S., Shimizu, H. and Ohta, K.: Overview of the 1990–1995 eruption at Unzen Volcano, *J.*  
892 *Volcanol. Geotherm. Res.*, 89 (1), 1-22, 1999.
- 893
- 894 Navarro-Ochoa, C., Gavilanes-Ruiz, A. Cortès-Cortès, A.: Movement and emplacement of lava  
895 flows at Volcán de Colima, México: November 1998–February 1999, *J. Volcanol.*  
896 *Geotherm. Res.*, 117 (1), 155-167, 2002.
- 897
- 898 Nicholson, R.S., Gardner, J.E., and Neal, C.A.: Variations in eruption style during the 1931 A.D.  
eruption of Aniakchak volcano, Alaska, *J. Volcanol. Geotherm. Res.*, 207, 69–82, 2011.
- 899
- 900 Norini, G., Capra, L., Gropelli, G., Agliardi, F., Pola, A., and Cortès, A.: Structural architecture of  
the Colima Volcanic Complex, *J. Geophys. Res.*, 115, B12209, 2010.
- 901
- 902 Odbert, H.M. and Wadge, G.: Time series analysis of lava flux. *J. Volcanol. Geotherm. Res.*,  
903 188(4), 305-314, 2009.
- 904
- 905 Ozerov, A., Ispolatov, I. and Lees, J.: Modeling strombolian eruptions of Karymsky volcano,  
906 Kamchatka, Russia, *J. Volcanol. Geotherm. Res.*, 122 (3), 265-280, 2003.
- 907
- 908 Ramsey, M.S. and Harris, A.J.L.: Volcanology 2020: how will thermal remote sensing of  
909 volcanic surface activity evolve over the next decade? *J. Volcanol. Geotherm. Res.*,  
910 <http://dx.doi.org/10.1016/j.jvolgeores.2012.05.011>, 2012.
- 911
- 912 Reyes-Dávila, G.A., Arámbula-Mendoza, R., Espinasa-Pereña, P., Pankhurst, M.J., Navarro-  
913 Ochoa, C., Savov, I. and Domínguez-Reyes, T.: Volcán de Colima dome collapse of  
914 July, 2015 and associated pyroclastic density currents, *J. Volcanol. Geotherm. Res.*, 320,  
915 100-106, 2016.
- 916
- 917 Reubi, O. and Blundy, J.: Assimilation of Plutonic roots, formation of high-K exotic melt  
918 inclusions and genesis of andesitic magmas at Volcán De Colima, Mexico, *J. Petrol.* 49, 12,  
919 2221–2243, 2008.
- 920
- 921 Reubi, O., Blundy, J. and Varley, N.: Volatiles contents, degassing and crystallisation of  
922 intermediate magmas at Volcán de Colima, Mexico, inferred from melt inclusions.  
*Contr. Mineral. Petrol.*, 165(6), 1087-1106, 2013.

- 923 Reubi, O., Sims, K.W., Varley, N., Reagan, M. and Eikenberg, J.: Timescales of degassing and  
 924 conduit dynamics inferred from  $^{210}\text{Pb}$ – $^{226}\text{Ra}$  disequilibria in Volcan de Colima 1998–  
 925 2010 andesitic magmas. *Geol. Soc., London, Sp. Publ.*, 422, SP422-5, 2015.  
 926
- 927 Roverato, M., Capra, L., Sulpizio, R., Norini, G.: Stratigraphic reconstruction of two debris  
 928 avalanche deposits at Colima Volcano (Mexico): insights into pre-failure conditions and  
 929 climate influence. *Journal of Volcanology and Geothermal Research*, 207(1-2), 33-46, 2011.  
 930
- 931 Salzer, J.T., Nikkhoo, M., Walter, T.R., Sudhaus, H., Reyes-Dávila, G., Bretón, M. and Arámbula,  
 932 R.: Satellite radar data reveal short-term pre-explosive displacements and a complex conduit  
 933 system at Volcán de Colima, Mexico, *Frontiers in Earth Sci.*, 2, 12, 2014.  
 934
- 935 Saucedo, R., Macias, J.L., Sheridan, M.F., Bursik, M.I., Komorowski, J.C.: Modeling of  
 936 pyroclastic flows of Colima Volcano, Mexico: implications for hazard assessment, *J.*  
 937 *Volcanol. Geotherm. Res.*, 139 (1–2), 103–115, 2005.  
 938
- 939 Saucedo, R., J.L. Macías, J.C. Gavilanes, J.L. Arce, J.C. Komorowski, J.E. Gardner, and G.  
 940 Valdez-Moreno, G.: Eyewitness, stratigraphy, chemistry, and eruptive dynamics of the  
 941 1913 Plinian eruption of Volcán de Colima, México, *J. Volcanol. Geotherm. Res.*, 191(3),  
 942 149-166, 2010.  
 943
- 944 Savov, I.P., Luhr, J.F. and Navarro-Ochoa, C.; Petrology and geochemistry of lava and ash  
 945 erupted from Volcan Colima, Mexico, during 1998-2005, *J. Volcanol. Geotherm. Res.*, 174,  
 946 241–256, 2008.  
 947
- 948 Siswamidjyo, S., Suryo, I. and Yokoyama, I.: Magma eruption rates of Merapi volcano,  
 949 Central Java, Indonesia during one century (1890–1992), *B. Volcanol.*, 57 (2), 111-116,  
 950 1995.  
 951
- 952 Sparks, R.S.J.: Causes and consequences of pressurisation in lava dome eruptions, *Earth Planet. Sci.*  
 953 *Lett.*, 150 (3-4), 177-189, 1997.  
 954
- 955 Sparks, R.S.J. and Young, S.R.: The eruption of Soufrière Hills volcano, Montserrat (1995–1999):  
 956 Overview of scientific results, in *The Eruption of the Soufrière Hills Volcano, Montserrat*  
 957 *from 1995 to 1999*, *Geol. Soc. London Mem.*, 21, 45– 69, 2002.  
 958
- 959 Spica, Z., Pertou, M. and Legrand, D.: Anatomy of the Colima volcano magmatic system,  
 960 Mexico, *Earth Planet. Sci. Lett.*, 459, 1-13, 2017.  
 961
- 962 Sulpizio, R., Capra, L., Sarocchi, D., Saucedo, R., Gavilanes-Ruiz, J. C. and Varley, N.: Predicting  
 963 the block-and-ash flow inundation areas at Volcán de Colima (Colima, Mexico) based on  
 964 the present day (February 2010) status. *J. Volcanol. Geotherm. Res.*, 193(1-2), 49-66, 2010.  
 965
- 966 Swanson, D.A. and Holcomb, R.T.: Regularities in growth of the Mount St. Helens dacite  
 967 dome, 1980–1986, in *Lava Flows and Domes: Emplacement Mechanisms and Hazard*  
 968 *Implications*, 3-24, 1990.  
 969
- 970 Thiele, S.T., Varley, N. and James, M.R.: Thermal photogrammetric imaging: A new technique for  
 971 monitoring dome eruptions, *J. Volcanol. Geotherm. Res.*, 337, 140-145, 2017.  
 972
- 973 Trauth, M.: *MATLAB Recipes for Earth Sciences*, 1st ed. Springer-Verlag, Berlin Heidelberg,  
 974 2006.

- 975 Torrence, C. and Compo, G.P.: A practical guide to wavelet analysis. *Bulletin of the American*  
 976 *Meteorological society*, 79(1), 61-78, 1998.
- 977
- 978 Varley, N., Arámbula-Mendoza, R., Reyes-Dávila, G., Stevenson, J., Harwood, R.: Long-  
 979 period seismicity during magma movement at Volcán de Colima, B. *Volcanol.*, 72, 1093–  
 980 1107. <http://dx.doi.org/10.1007/s00445-010-0390-7>, 2010a.
- 981
- 982 Varley, N., Arámbula-Mendoza, R., Reyes-Reyes-Dávila, G., Sanderson, R., Stevenson, J.:  
 983 Generation of Vulcanian activity and long-period seismicity at Volcan de Colima, Mexico.  
 984 *J. Volcanol. Geotherm. Res.*, 198, 45–56, 2010b.
- 985 Varley, N: La evolución de la actividad reciente del Volcán de Colima, webseminar, Unión  
 986 Geofísica Mexicana A.C., 2015.
- 987
- 988 Vila, J., Macià, R., Kumar, D., Ortiz, R., Moreno, H., Correig, A.: Analysis of the unrest of active  
 989 volcanoes using variations of the base level noise seismic spectrum. *J. Volcanol. Geotherm.*  
 990 *Res.* 153, 11–20, 2006.
- 991 Voight, B., Hoblitt, R.P., Clarke, A.B., Lockhart, A. Miller, L. Lynch and McMahon, J.:  
 992 Remarkable cyclic ground deformation monitored in real-time on Montserrat, and its use  
 993 in eruption forecasting, *Geophys. Res. Lett.*, 25 (18), 3405-3408, 1998.
- 994
- 995 Voight, B., Sparks, R.S.J., Miller, A.D., Stewart, R.C., Hoblitt, R.P., Clarke, A. and Cole, P.:  
 996 Magma flow instability and cyclic activity at Soufriere Hills volcano, Montserrat,  
 997 british west indies, *Science*, 283 (5405), 1138-1142, 1999.
- 998
- 999 Voight, B., Constantine, E.K., Siswamidjono, S. and Torley, R.: Historical eruptions of Merapi  
 1000 volcano, central Java, Indonesia, 1768–1998, *J. Volcanol. Geotherm. Res.*, 100 (1), 69-138,  
 1001 2000.
- 1002
- 1003 Wadge, G., Dorta, D.O. and Cole, P.D.: The magma budget of Volcán Arenal, Costa Rica  
 1004 from 1980 to 2004, *J. Volcanol. Geotherm. Res.*, 157 (1), 60-74, 2006.
- 1005
- 1006 Wadge, G., Herd, R., Ryan, G., Calder, E.S. and Komorowski, J.C.: Lava production at Soufrière  
 1007 Hills Volcano, Montserrat: 1995–2009, *Geophys. Res. Lett.*, 37 (19), 2010.
- 1008
- 1009 Watts, R.B., Herd, R.A., Sparks, R.S.J. and Young, S.R.: Growth patterns and emplacement of the  
 1010 andesitic lava dome at Soufriere Hills Volcano, Montserrat, *Geol. Soc. Lond. Mem.* 21(1),  
 1011 115-152, 2002.
- 1012
- 1013 Weng, H. and Lau, K.M.: Wavelets, period doubling, and time-frequency localization with  
 1014 application to organization of convection over the tropical western Pacific. *J. Atmos. Sci.*,  
 1015 51, 2523–2541, 1994.
- 1016 Wolpert, R., Ogburn, L. and Calder, E.S.: The longevity of lava dome eruptions. *Journal of*  
 1017 *Geophysical Research: Solid Earth*, 121(2), 676-686, 2016.
- 1018
- 1019 Wylie, J.J., Voight, B. and Whitehead, J.A.: Instability of magma flow from volatile dependent  
 1020 viscosity, *Science*, 285, 1883–1885 1999.



L021 Zobin, V.M., Orozco-Rojas, J., Reyes-Dávila, G.A. and Navarro-Ochoa, C.: Seismicity of an  
L022 andesitic volcano during block-lava effusion: Volcán de Colima, México, November 1998–  
L023 January 1999, Bull. Volcanol. 67 (7), 679-688, 2005.  
L024  
L025 Zobin, V.M., Varley, N., González, M., Orozco, J., Reyes, G.A., Navarro-Ochoa, C. and M.  
L026 Bretón: Monitoring the 2004 andesitic block-lava extrusion at Volcán de Colima,  
L027 México from seismic activity and SO<sub>2</sub> emission, J. Volcanol. Geotherm. Res., 177 (2), 367-  
L028 377, 2008.  
L029  
L030 Zobin, V.M., R. Arámbula, R., Bretón, M., Reyes, G., I. Plascencia, I., Navarro-Ochoa, C. and  
L031 Martínez, A.: Dynamics of the January 2013–June 2014 explosive-effusive episode in the  
L032 eruption of Volcán de Colima, México: insights from seismic and video monitoring, Bull.  
L033 Volcanol. 77(4), 31, 2015.  
L034  
L035  
L036  
L037  
L038  
L039  
L040  
L041  
L042  
L043  
L044  
L045 **Tables**  
L046

Table 1: Input parameters used in numerical simulations.

Notation	Description	Value
$c_o$	Concentration of dissolved gas (wt.%)	5-6
$C_f$	Solubility coefficient (Pa <sup>-1/2</sup> )	$4.1 \times 10^{-6}$
$C_m$	Specific heat (J kg <sup>-1</sup> K <sup>-1</sup> )	$1.2 \times 10^3$
$I_0$	Max nucleation rate (m <sup>-3</sup> s <sup>-1</sup> )	$3 \times 10^{10}$
$L_*$	Latent heat of crystallization (J kg <sup>-1</sup> )	$3.5 \times 10^5$
$\mu_g$	Gas viscosity (Pa s)	$1.5 \times 10^{-5}$
$\rho_m$	Density of the melt phase (kg m <sup>-3</sup> )	2300-2500
$\rho_c$	Density of the crystal (kg m <sup>-3</sup> )	2700-2800
$T_{ch}$	Magma chamber temperature (K)	1150
$P_{ch}$	Magma chamber pressure (MPa)	130 – 210
$\beta_{ch*}$	Magma chamber crystal content	0.35-0.45
$\mu$	Magma viscosity (Pa s)	$3.7 \times 10^5$
$\rho_r$	Host rock density (kg m <sup>-3</sup> )	2600
$G$	Host rock rigidity (GPa)	6
$\nu$	Poisson's ratio	0.25
$\varepsilon$		8.6

*Conduit geometry parameters using a single magma chamber model*

$D$	Diameter of the cylindrical conduit	30-40
$L_T$	Dyke-cylinder transition depth (m)	1300-500
$2a$	Dyke width (m)	200 – 600
$2b$	Dyke thickness (m)	4-40
$L$	Magma chamber depth (top) (m)	6000-6500
$V_{ch}$	Magma chamber volume (km <sup>3</sup> )	20-50
$AR$	Magma chamber aspect ratio	1-2
$Q_{in,s}$	Influx into the shallow magma chamber (m <sup>3</sup> s <sup>-1</sup> )	0.01-3.5

*Parameters used for simulations carried out with dual magma chamber model*

*Deep magma chamber*

$2a_{od}$	Deeper dyke width (m)	200 – 3000
$L_0$	Deep magma chamber depth (top) (m)	15000
$AR_d$	Deep magma chamber aspect ratio	1-2
$V_{chd}$	Deep magma chamber volume (km <sup>3</sup> )	550-750
$\Delta P$	Deep magma chamber overpressure (MPa)	20
$Q_{in,d}$	Influx into the shallow magma chamber (m <sup>3</sup> s <sup>-1</sup> )	1-3

L047 **Figures Captions**

L048 **Fig. 1.** (a) Digital elevation model of the Colima Volcanic Complex (NC = Nevado de Colima  
L049 volcano; FC = Fuego de Colima volcano) and Colima Rift with the main tectonic and volcano-  
L050 tectonic structures (modified from Norini et al. 2010). In the inset, the location of the Colima  
L051 Volcanic Complex (CVC) within the Trans-Mexican Volcanic Belt (TMVB) is shown in the frame  
L052 of the subduction-type geodynamic setting of Central America. (b) Schematic view of the conduit  
L053 feeding system framework used for numerical simulations (modified after Melnik and Costa, 2014).

L054 **Fig. 2.** Dataset about the averaged discharge rates of Fuego de Colima during 1998-2018, derived  
L055 by the MIROVA thermal data (black points) and published data (blue crosses) (Navarro-Ochoa et  
L056 al., 2002; Zobin et al., 2005; Reubi et al 2013; Mueller et al., 2013; Varley, 2015; Reyes-Dávila et  
L057 al., 2016; Thiele et al., 2017; GVP, 2002-2017). Values  $> 0.1$  (m<sup>3</sup> s<sup>-1</sup>) are considered to be as “high”  
L058 (dark blue area) and values  $< 0.1$  (m<sup>3</sup> s<sup>-1</sup>) as “low” discharge rate (light blue area). The 0.01 (m<sup>3</sup> s<sup>-1</sup>)  
L059 is the threshold under which the MIROVA system does not provide reliable data (blue line); (a)  
L060 Weekly average discharge rates. The boxes contain symbols of volcanological observations  
L061 reported in literature; (b) Monthly average discharge rates; (c) Yearly average discharge rates.

L062 **Fig. 3.** (a) Local wavelet power spectrum normalized by  $1/\sigma^2$  ( $\sigma^2$  in  $(\text{m}^3 \text{s}^{-1})^2$ ). The left axis is the  
 L063 period (in years). The bottom axis is time (in years). The shaded contours are at normalized  
 L064 variances of 0.5, 1, 2, and 4  $(\text{m}^3 \text{s}^{-1})^2$ . The black thick contour encloses regions of greater than 95%  
 L065 confidence for a red-noise process with a lag-1 coefficient of 0.72. It shows three orders of  
 L066 periodicities of: long-term (ca. 1.5-2.5 years), intermediate-term (ca. 5-10 months) during 2002-  
 L067 2006 and 2013-2016, and short-term (ca. 2.5-5 weeks) during 2001-2006 and 2011-2016. Blue line  
 L068 indicates the “cone of influence” where edge effects become important outside it; (b) Global  
 L069 wavelet power spectrum. The green dotted line represents the best-fitting red noise spectrum at the  
 L070 95% confidence level.

L071 **Fig. 4.** Results of numerical simulations. The physical framework of the conduit feeding system has  
 L072 deep and shallow chambers connected to surface via vertical elastic dykes evolving into non-elastic  
 L073 cylinder. The length of the shallow dyke  $L_{ds}$  is in the range of 6000-6500 m. The passage to cylinder  
 L074 conduit  $L_r$  occurs at ca. 1300-500 m below the cone. (a) Discharge rates vs. time considering the  
 L075 elasticity of the shallower dyke, with a width  $2a = 400$  m and thickness  $2b = 2$  m. The cylinder  
 L076 diameter  $D = 30$  m. Two cases are shown: *i*) constant pressure (blue line) and *ii*) constant influx rate  
 L077 at the source region of the dyke, providing different periodicities of 16 and 40 days, in good  
 L078 agreement with the short-term (weekly) periodicities observed in Fig. 3a; (b) Discharge rate vs. time  
 L079 using the single magma chamber model. The dyke width  $2a = 600$  and thickness  $2b = 4$  m. The  
 L080 chamber has a volume  $V_{ch} = 30 \text{ km}^3$ , receiving a constant influx  $Q_{in,s} = 2.3 (\text{m}^3 \text{s}^{-1})$ ; Periodicity is of  
 L081 ca. 220 days, in good agreement with the intermediate-term (monthly) periodicities observed in Fig.  
 L082 3a; (c) Discharge rate vs. time using the dual magma chamber model. The aspect ratio of the  
 L083 shallow and deep chambers ( $AR_s - AR_d$ ) are both equal to 1.3 and 1.4, respectively. The upper  
 L084 feeding system has a chamber ( $V_{chs} = 30 \text{ km}^3$ ) connected to a dyke (width  $2a = 260$  m;  $2b = 4$  m)  
 L085 evolving into a cylinder ( $D = 30$  m) at  $L_r = 1000$  m. The shallow chamber is connected to the deep  
 L086 one ( $V_{chd} = 500 \text{ km}^3$ ) through a feeder dyke ( $2a_{od} = 500$  m). A constant  $Q_{in,d} = 2.3 (\text{m}^3 \text{s}^{-1})$  is  
 L087 injected from below. Periodicity is in the range of ca. 825 days, in good agreement with the long-  
 L088 term (yearly) periodicities observed in Fig. 3a.

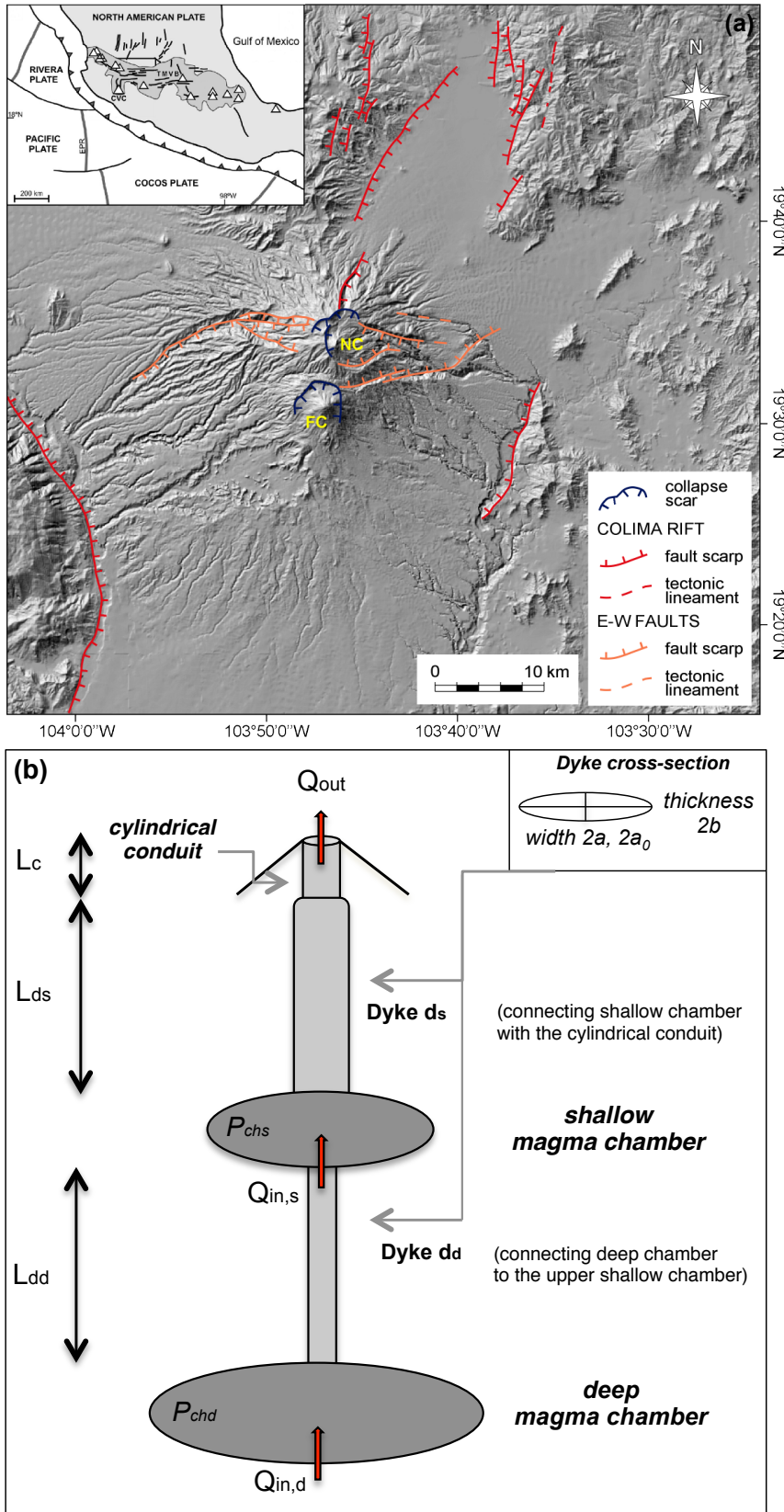
L089

L090

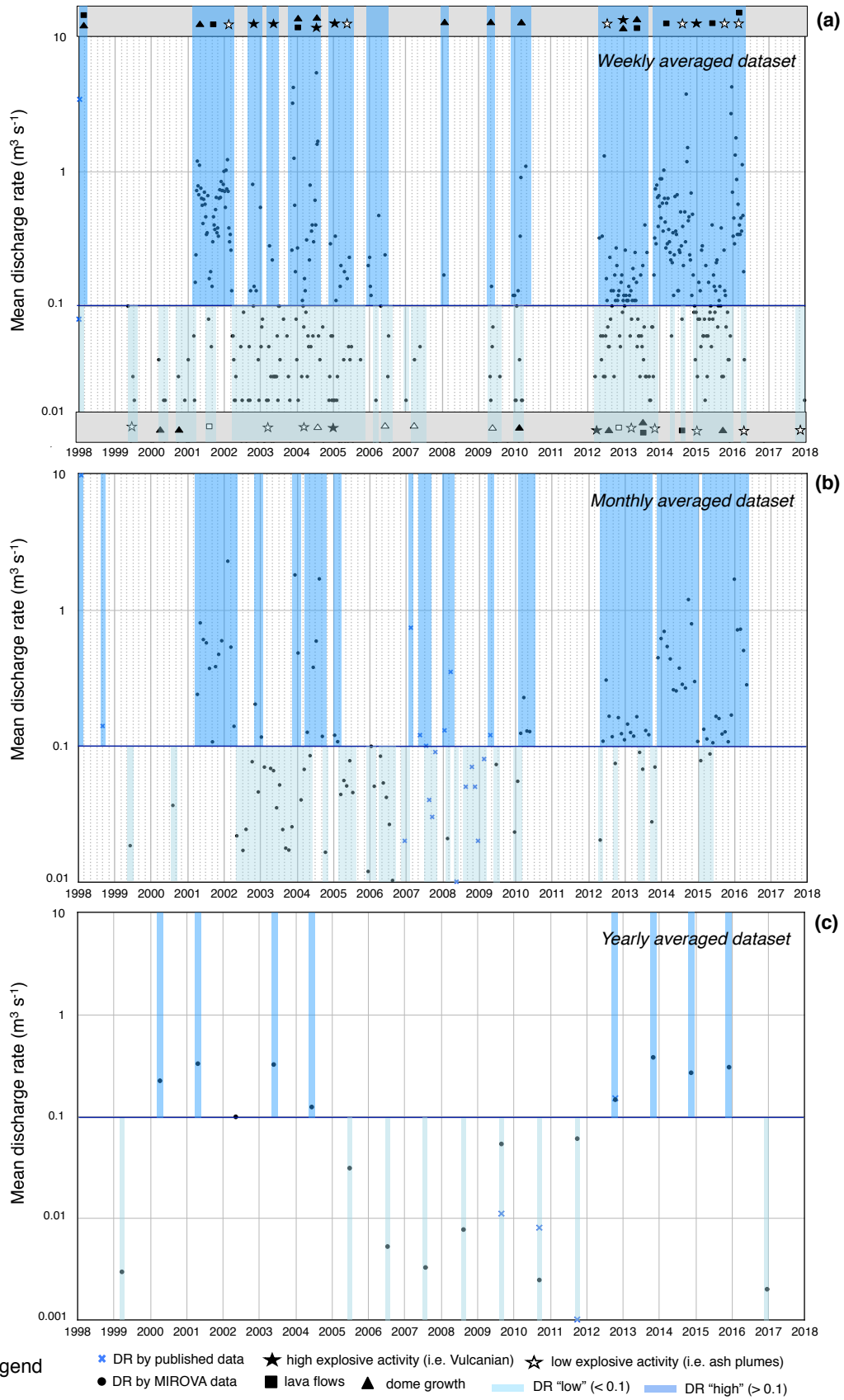
L091

L092

L093 Fig.1



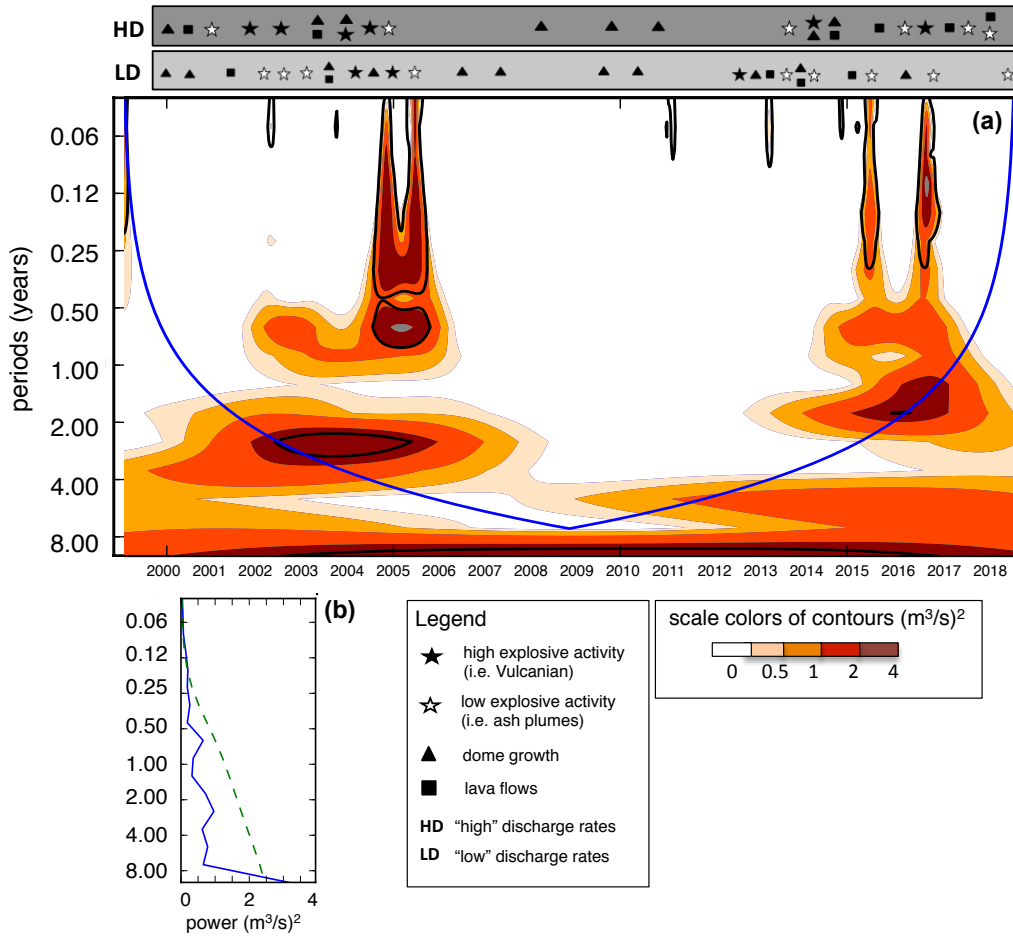
L094



L098

L099 **Fig.3**

L100



L101

L102

L103

L104

L105

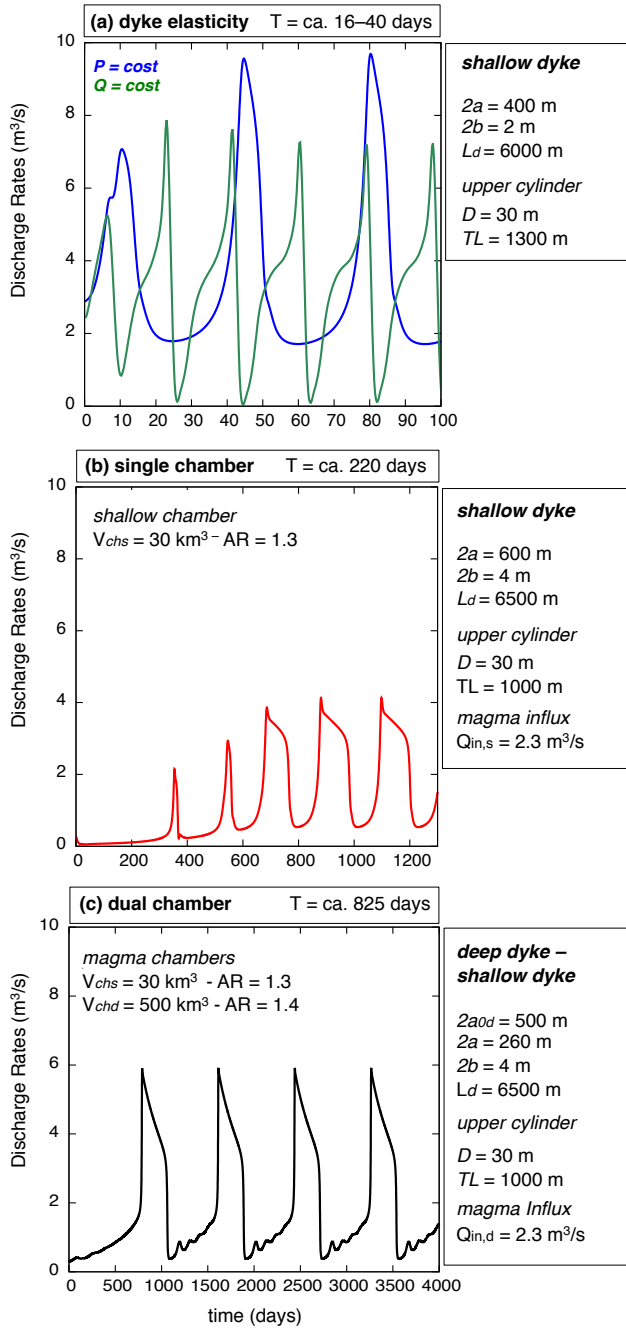
L106

L107

L108

L109

L110 Fig. 4



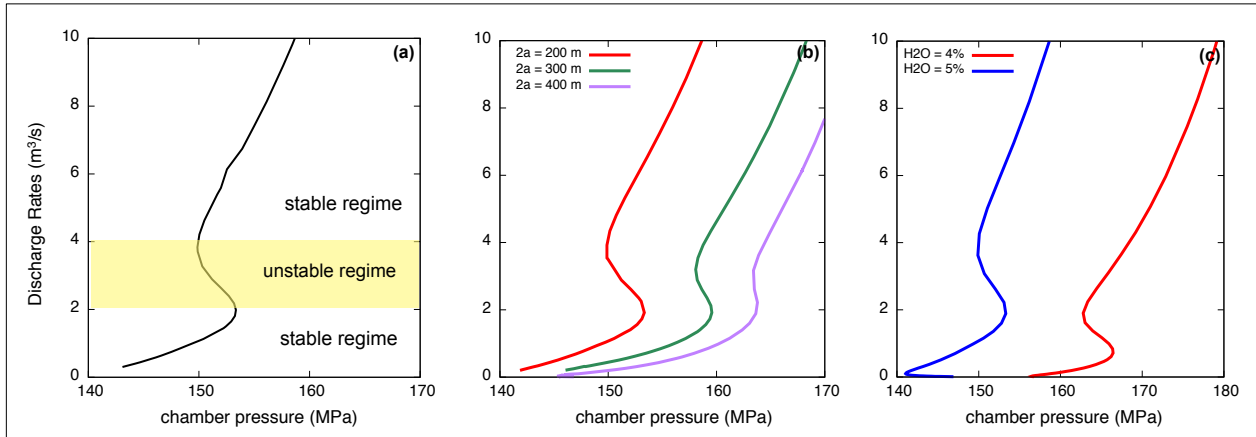
L111

L112

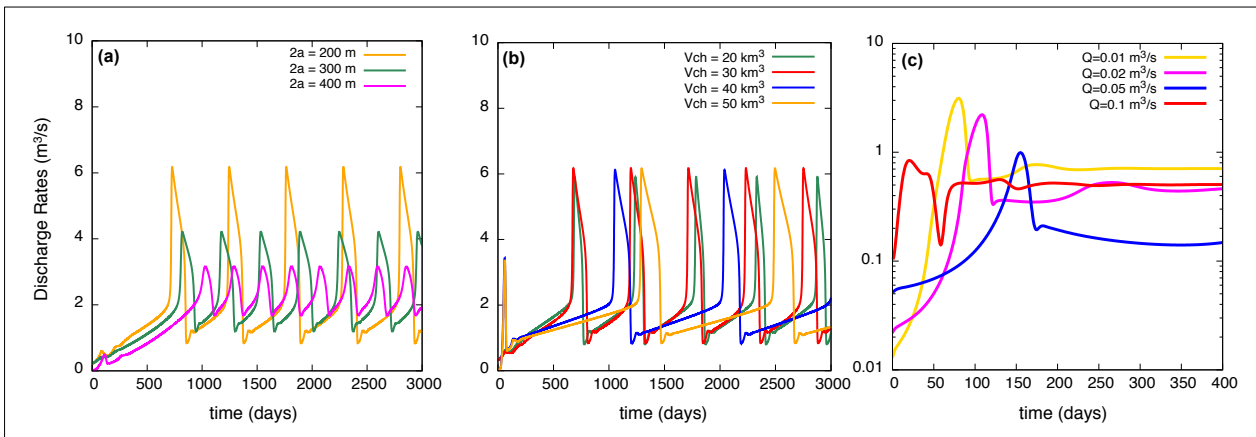
L113 **Appendix A1-A2**

L114

A1



A2



L115

L116

L117

L118

L119

L120

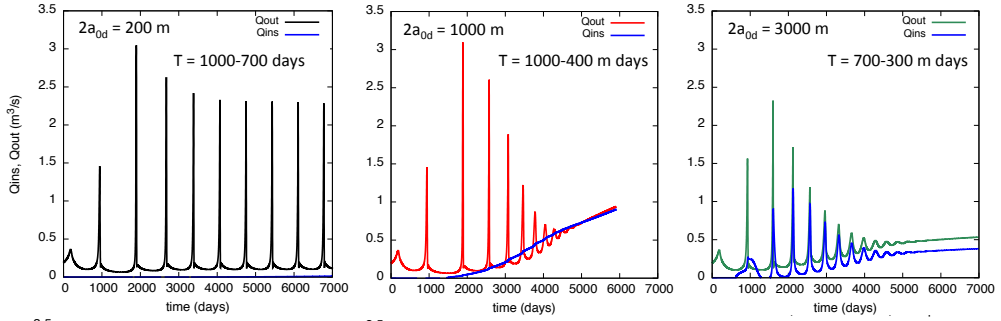
L121

L122

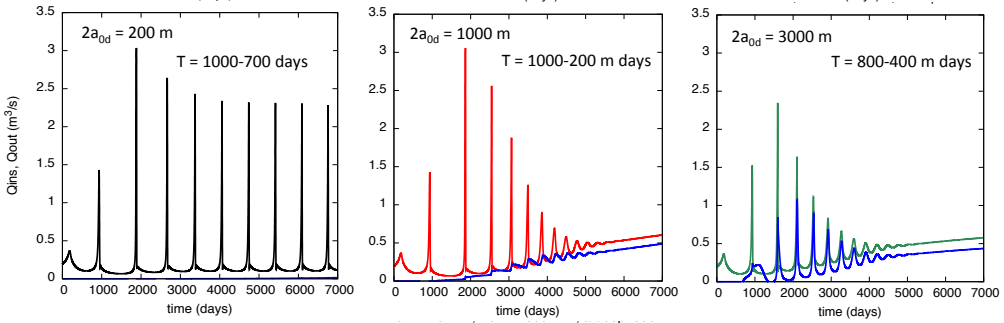


**Fixed parameters**  
 $V_{chs} = 40 \text{ km}^3$   
 $V_{chd} = 650 \text{ km}^3$

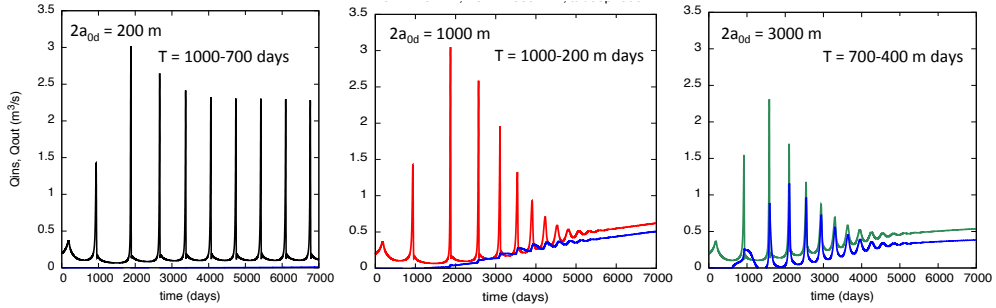
**Aspect Ratio**  
 $ARs = 1$   
 $ARd = 1$



**Aspect Ratio**  
 $ARs = 2$   
 $ARd = 1$

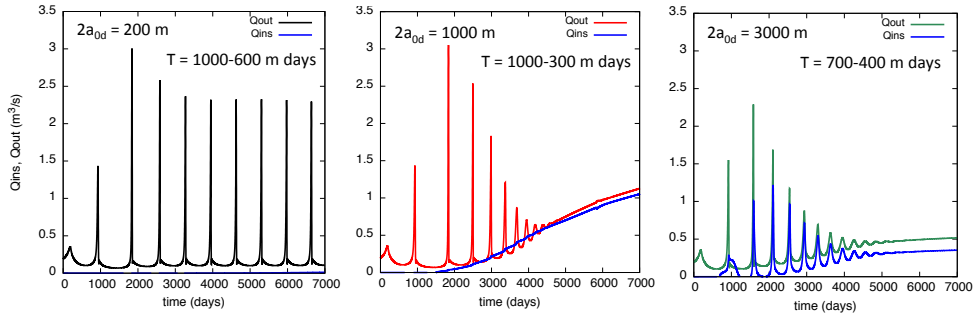


**Aspect Ratio**  
 $ARs = 2$   
 $ARd = 1.5$

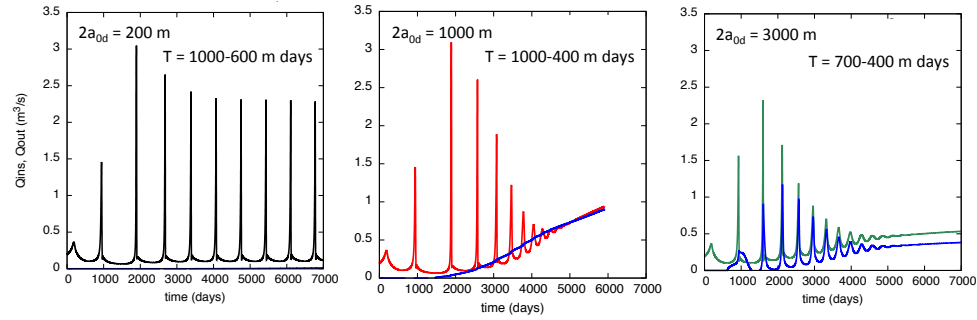


**Fixed parameters**  
 ARs = 1  
 ARd = 1  
 $V_{chd} = 650 \text{ km}^3$

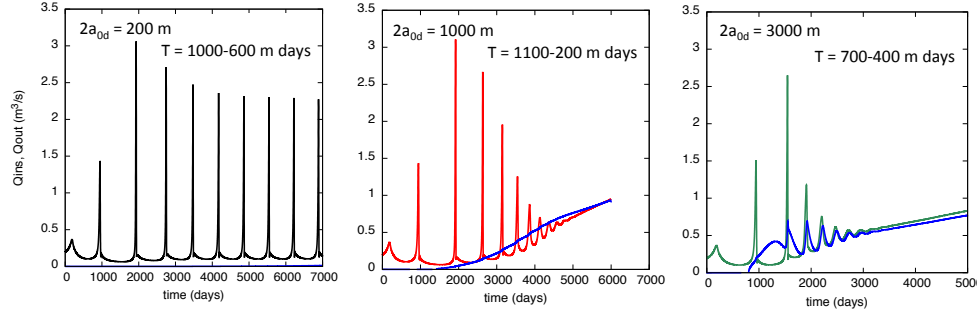
**Shallow Chamber Volume**  
 $V_{chs} = 30 \text{ km}^3$



**Shallow Chamber Volume**  
 $V_{chs} = 40 \text{ km}^3$

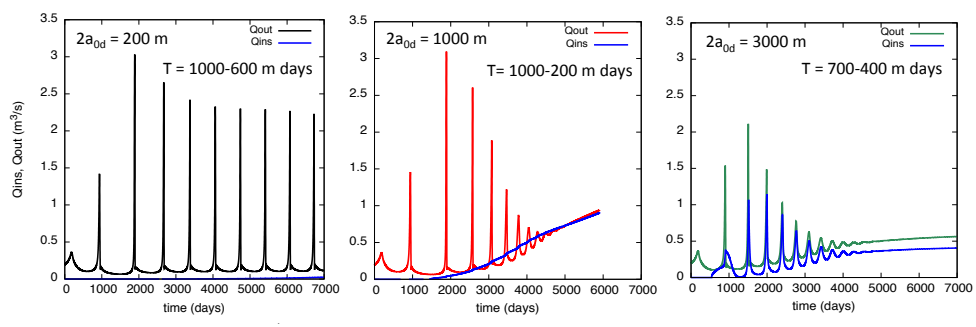


**Shallow Chamber Volume**  
 $V_{chs} = 50 \text{ km}^3$

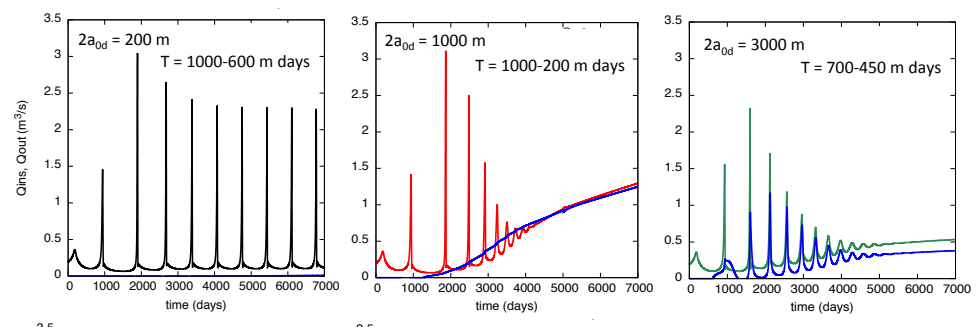


**Fixed parameters**  
 ARs = 1  
 ARd = 1  
 V<sub>chs</sub> = 40 km<sup>3</sup>

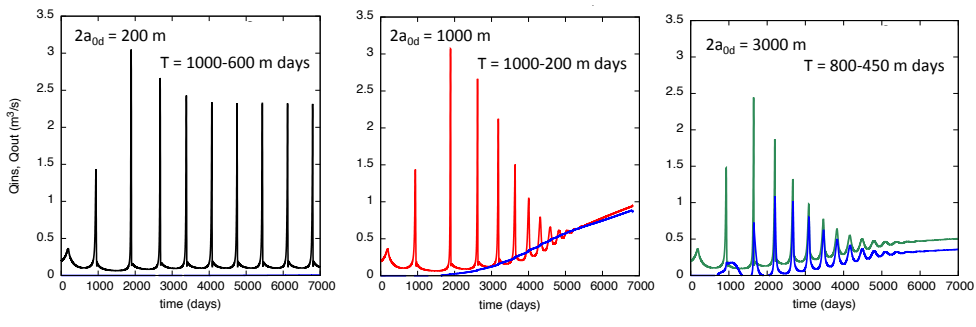
**Deeper Chamber Volume**  
 V<sub>chd</sub> = 550 km<sup>3</sup>



**Deeper Chamber Volume**  
 V<sub>chd</sub> = 650 km<sup>3</sup>



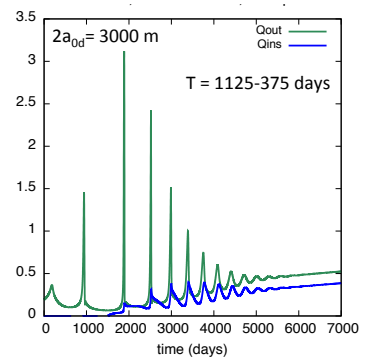
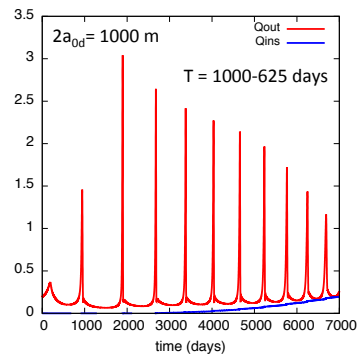
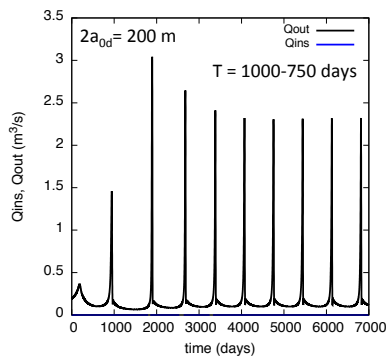
**Deeper Chamber Volume**  
 V<sub>chd</sub> = 750 km<sup>3</sup>



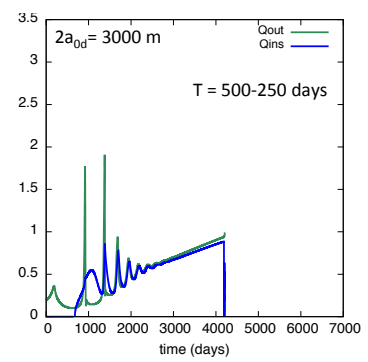
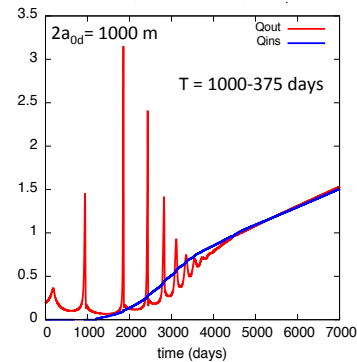
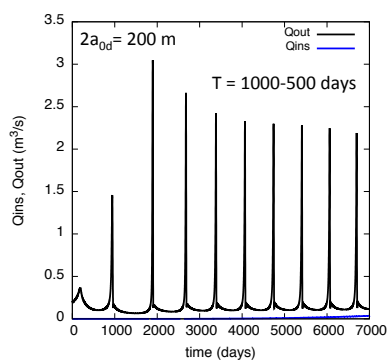
Fixed parameters : ARs = 1 ; ARd = 1; Vchd = 650 km<sup>3</sup> ; Vchs = 40 km<sup>3</sup>

4

▪  $Q_{in\_depth} = 1 \text{ m}^3/s$



▪  $Q_{in\_depth} = 3 \text{ m}^3/s$



L128

L129

L130

L131

L132

L133

L134

L135

L136

L137

L138

